2011

Simulation and Experiment for Induction Motor Control Strategies

Zhi Shang
University of Windsor

Simulation and Experiment for Induction Motor Control Strategies

by

Zhi SHANG

A Thesis

Submitted to the Faculty of Graduate Studies

through Mechanical Engineering

in Partial Fulfillment of the Requirements for

the Degree of Master of Applied Science at the

University of Windsor

Windsor, Ontario, Canada

2011

Simulation and Experiment for Induction Motor Control Strategies

by

Zhi SHANG

APPROVED BY:

Dr. J. Johrendt, Department Reader

Department of Mechanical, Automotive & Material Engineering

Dr. H. Wu, Outside Department Reader

Department of Electrical and Computer Engineering

Dr. B. Zhou, Advisor

Department of Mechanical, Automotive & Material Engineering

Dr. C. Novak, Chair of Defense

Department of Mechanical, Automotive & Material Engineering

AUTHOR'S DECLARATION OF ORIGINALITY

I hereby certify that I am the sole author of this thesis and that no part of this thesis has been published or submitted for publication.

I certify that, to the best of my knowledge, my thesis does not infringe upon anyone's copyright nor violate any proprietary rights and that any ideas, techniques, quotations, or any other material from the work of other people included in my thesis, published or otherwise, are fully acknowledged in accordance with the standard referencing practices. Furthermore, to the extent that I have included copyrighted material that surpasses the bounds of fair dealing within the meaning of the Canada Copyright Act, I certify that I have obtained a written permission from the copyright owner(s) to include such material(s) in my thesis and have included copies of such copyright clearances to my appendix.

I declare that this is a true copy of my thesis, including any final revisions, as approved by my thesis committee and the Graduate Studies office, and that this thesis has not been submitted for a higher degree to any other University or Institution.

ABSTRACT

The Induction motor has been widely used in industry and is considered as the best candidate for electrical vehicle (EV) applications due to its advantages such as: simple design, ruggedness, and easy maintenance. However, the precise control of induction motor is not easy to achieve, because it is a complicated nonlinear system, the electric rotor variables are not measurable directly, and the physical parameters could change in different operating conditions. So the control of an induction motor becomes a critical issue, especially for the EV applications in which both fast transient responses and excellent steady state speed performance are required.

Three induction motor control algorithms (field orientation control, conventional direct torque control, and stator flux orientated sensorless direct torque control) are introduced in this thesis and a specific comparison is given among three of them. The main focus of this work is to design an induction motor control system using the three algorithms mentioned above, to analyze the performances of different control methods, and to validate these algorithms experimentally, comparing the simulation and experimental results.

DEDICATION

To my parents, my teachers and anyone who ever shared their knowledge with me.

ACKNOWLEDGEMENTS

I wish to express my sincere gratitude to my supervisor Dr. B. Zhou, who has been a constant source of guidance, support and encouragement throughout my graduate studies. His extensive knowledge, rigorous research attitude, diligent working and creative thinking have inspired me and will definitely benefit my future career.

My gratitude should also be given to Dr. J. Johrendt and Dr. H. Wu for serving as my committee members, giving me valuable suggestions and taking the time to revise my thesis. I would like to dedicate all my thanks to them.

The experimental part of this project was the most challenging part. I could not have done this without the help from the technicians in Mechanical Engineering Department: Mr. Andy Jenner and Mr. Patrick Seguin, also the technician in Electrical Engineering Department: Mr. Frank Cicchello. I would like to thank them with enormous appreciation for their help and advice.

I also would like to express my thanks to Mr. Ahmad Fadel, Mr. Rui Hu, and Mr. Esmaeil Navaei Alvar. It has been a great pleasure studying and working with them. The discussions, comments and suggestions they gave to me allowed me to improve my research in many aspects.

Finally I would like to thank my parents for their love, support and sacrifices. They are the strength behind my strive for success.

TABLE OF CONTENTS

LIST OF FIGURES

LIST OF SYMBOLS

α	Axis of stationary frame
β	Axis of stationary frame
d	Axis of rotating frame
q	Axis of rotating frame
n_{sync}	Synchronous speed in revolutions per minute
f_e	Frequency of the power source
P	The number of poles
n_{slip}	Slip speed
n_m	Mechanical shaft speed of the motor
s	Slip ratio
i_s	Stator current
i_r	Rotor current
$i_{a,b,c}$	Three phase current
Ψ_s	Stator flux
Ψ_r	Rotor flux
Ψ_m	Mutual flux
$i_{\alpha s}$	Stator current component in Alfa-axis
$i_{\beta s}$	Stator current component in Beta-axis
$i_{\alpha r}$	Rotor current component in Alfa-axis
$i_{\beta r}$	Rotor current component in Beta-axis
i_{ds}	Stator current component in d-axis
i_{qs}	Stator current component in q-axis
i_{dr}	Rotor current component in d-axis
i_{qr}	Rotor current component in q-axis
R	Resistance
R_s	Stator resistance

R_r	Rotor resistance
u_s	Stator voltage
$u_{\alpha s}$	Stator voltage component in Alfa-axis
$u_{\beta s}$	Stator voltage component in Beta-axis
p	Differential operator d/dt
L_s	Stator inductance
L_r	Rotor inductance
L_m	Mutual inductance
l	Inductance
ω_r	Rotor mechanical angular velocity
ω_e	Synchronous angular velocity
ω_{sl}	Slip angular velocity
θ_e	Synchronous angle
θ_{er}	Rotor flux angle in synchronous frame
θ_m	Phase angle of voltage vector u_m
θ_s	Stator flux angle
θ	Angle between rotor flux and stator flux
T_e	Electromagnetic torque
T_L	Load torque
B_s	Stator magnetic flux density
B_r	Rotor magnetic flux density
$K_0 \sim K_6$	Torque constant
J	Rotor's moment of inertia
V_{dc}	DC main bus Voltage
$V_{an,bn,cn}$	Phase voltage
$V_{ab,bc,ca}$	Line to line voltage
$S_{1,3,5}$	Switching variable vectors
$V_0 \sim V_7$	Space voltage vectors
T_r	Rotor time constant (s) $T_r = L_r/R_r$

S_{Ψ}	Flux flag
ΔE_{Ψ}	Flux error
Ψ_g	Flux hysteresis controller boundary
S_{Te}	Torque flag
ΔE_T	Torque error
T_g	Torque hysteresis controller boundary
S(K)	Sector number, K=1~6
$*$, ref	Reference values
^	Estimated values

CHAPTER I. INTRODUCTION

1.1 Background

The development of internal combustion engine vehicles is one of the greatest achievements in the automotive industry for the past a few centuries. Automobiles have made great contributions to the growth of modern technology, economy, even cultures by satisfying many of the needs for mobility in our daily life.

However, the large numbers of automobiles which are being used all around the world have caused serious problems for the environment and human life. Air pollution, global warming, and the rapid depletion of the earth's petroleum resources are now problems of primary concern. The environmental issues and oil crisis compel people to develop clean, efficient vehicles solutions for urban transportation.

In the past a few decades, lots of research and development activities related to the automotive industry started emphasizing the development of clean, low/zero emission, and high efficiency transportation. So electric vehicles (EVs), hybrid electric vehicles (HEVs), and fuel cell vehicles became popular again and have been typically proposed to replace conventional vehicles in the near future. The electric vehicle is the first consideration for its zero emissions feature [1, 2].

1.2 Power Plant Characteristics

For vehicular applications, the ideal performance characteristic of a power plant is a constant power output over the full speed range. Consequently, the torque varies with speed hyperbolically as shown in Figure 1 [2, 3]. With this ideal profile, the maximum power of the power plant will be available at any vehicle speed, therefore yielding the optimal vehicle performance [2].

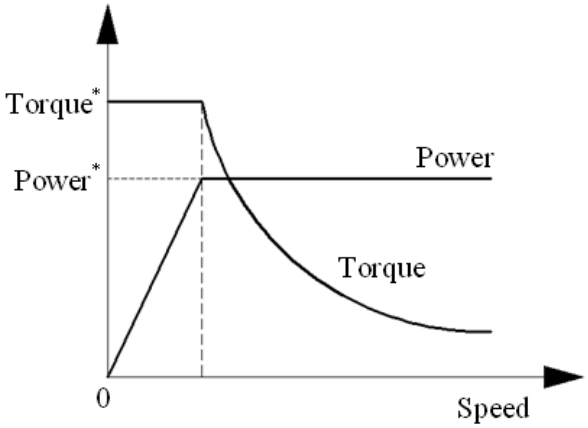

Figure 1: Ideal performance characteristics for a vehicle traction power plant

The most commonly used power plants for vehicles are no doubt the internal combustion engine. The typical characteristics of an internal combustion engine are shown in Figure 2[2]. Obviously, it is far from the ideal torque–speed profile curve. At the idle speed region, it operates in a smooth condition, but the maximum torque is achieved at an intermediate speed. With the speed further increasing, the torque decreases.

Instead of occurring at the very beginning, the maximum power happens at a high speed. Beyond this speed, the engine power decreases. Furthermore, the internal combustion engine has a relatively flat torque–speed profile, as compared with an ideal power plant shown in Figure 2. Therefore, a multi-gear transmission is commonly employed to modify the torque-speed profile, as shown in Figure 3 [2].

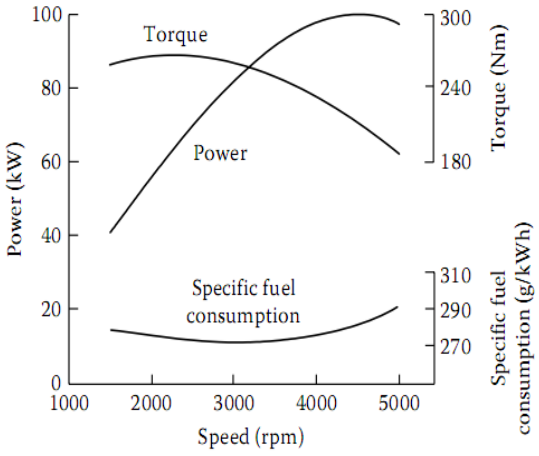

Figure 2: Typical characteristics of a gasoline engine [2]

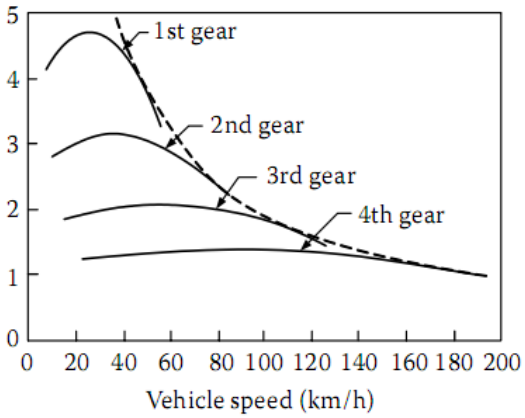

Figure 3: A multi-gear transmission vehicle gear ratio vs. speed [2]

The electric motor is another candidate as a vehicle power plant, and becoming more and more important with the rapid development of electric and hybrid electric vehicles.

Motors are the work horses of electric vehicles drive systems. An electric motor converts electrical energy from the energy storage unit to mechanical energy that drives the wheels of the vehicle. In the traditional vehicle case, the engine must ramp up before full torque can be provided [2]; however, in the case of electric motor, the full torque could be provided at low speed ranges [3]. This characteristic is very important; it gives the vehicle an excellent acceleration at the beginning. Also, other important characteristics of the motor include good control abilities, fault tolerance abilities, and high efficiency [4].

The speed–torque characteristics of electric motors are much closer to the ideal one, as shown in Figure 4 [2]. The speed starts from zero and generally increases to its base value. During this process, the voltage increases to its rated value as well, and the flux remains constant [3]. A constant torque is generated in this speed range from zero to base speed. Beyond the base speed, the voltage remains as a constant and the output power will also remain as a constant. Thus, the output torque declines hyperbolically with the increasing speed. Since the speed–torque profile of an electric

motor is close to the ideal one, people only need to use a single-gear or double-gear transmission to modify the vehicle performance to receive their desired design requirements [2].

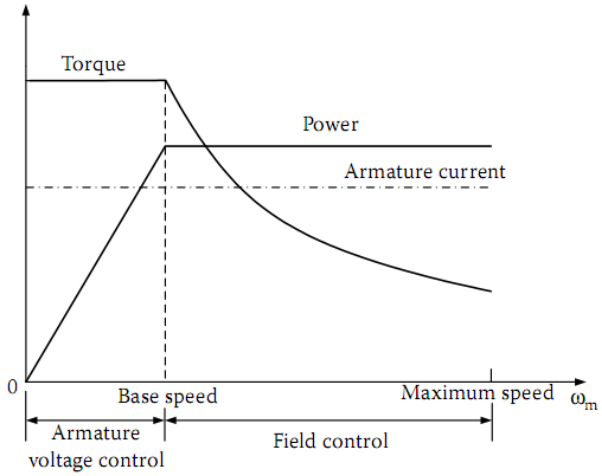

Figure 4: Typical characteristics of an electric motor [2]

1.3 Electric Motor

The motor drives for EVs can be classified into two groups, as shown in Figure 5:

- Commutator motors (also known as DC motors)
- Commutatorless motors (known as AC motors)

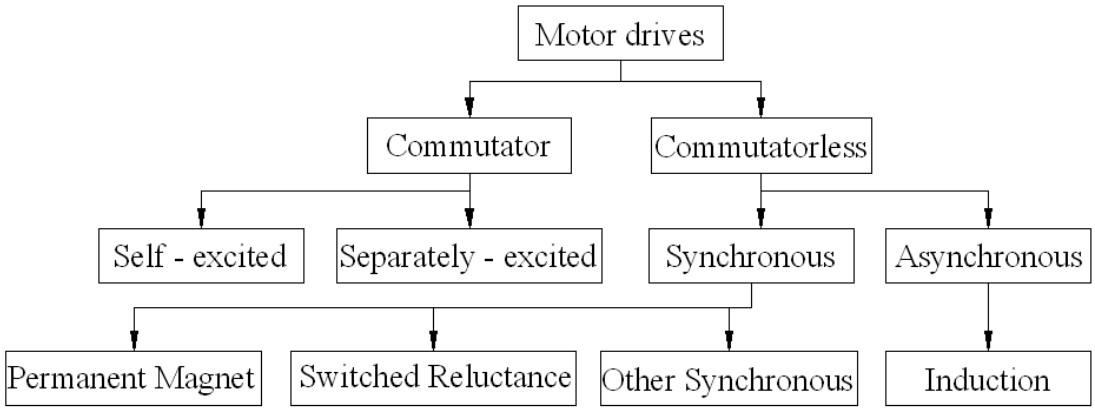

Figure 5: Classification of electric motor

1.3.1 Permanent Magnet Synchronous Motor (PMSM)

Instead of using the windings for the rotor, the PMSM's rotor is made of magnetic materials. So the operating principle of a PMSM is quite different from an induction

motor. The magnetic flux in a PMSM is generated from the magnetic materials on rotor. And absence of rotor windings gives PMSMs some advantages such as high efficiency and higher power density [5].

On the other side, the absence of field windings makes the flux weakening capability of PMSM's constrained, and eventually limits their speed ranges in the constant power region [6]. Also, the permanent magnet is very sensitive to the temperature, this will certainly lead to a demagnetization problem, and sometimes a special cooling system is necessary for a PMSM drive system.

Figure 6: Permanent magnet synchronous motors [7]

1.3.2 Switched Reluctance Motor

The switched reluctance motor is an electric motor which runs by reluctance torques [8]. It is another potential candidate due to some important features such as rugged structure, high power density, and insensitivity to high temperatures [9].

The wound field coils are fixed on the stator, but the rotor has no magnets or coils attached. When the opposite poles of the stator get energized, the rotor will become aligned. In order to achieve a full rotation of the motor, the windings must be energised in the right sequence [8].

The disadvantages of switched reluctance motors are high torque ripples, acoustic

noise, and instabilities caused by the energising sequence [9-11].

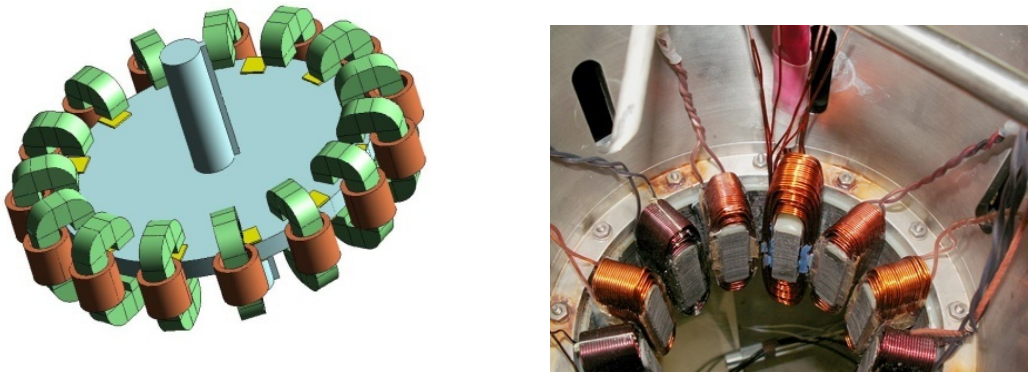

Figure 7: Switched reluctance motors [12]

1.3.3 Induction Motor

The induction motor is a type of AC motor; it is called an induction motor because the working principles are based on electromagnetic induction. The energy is transformed through the rotating magnetic fields in induction motor. The three-phase currents in the stator side create an electromagnetic field which interacts with the electromagnetic field in the rotor bars, and then the resultant torque will be produced by the Lorentz' law. Therefore, the electrical energy could be transformed into mechanical energy.

Induction motors are the preferred choice for industrial applications due to their rugged structure, low price and easy maintenance [13].

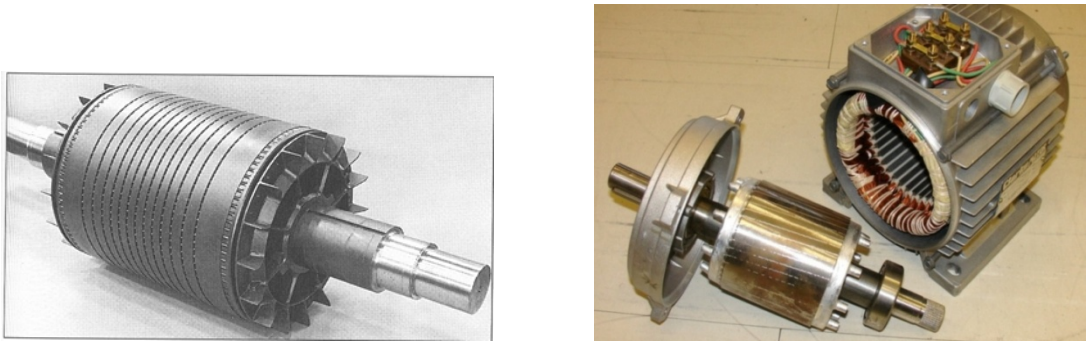

Figure 8: Induction motors [14]

1.3.4 Comparison of Three AC Motors

Table 1: Comparison among three AC motors [5-11]

Item	Induction Motor	PM Motor	SR Motor
Power density	Medium	High	Higher
Overload capacity (%)	300-500	300	300-500
Peak efficiency (%)	94-95	95-97	90
Load efficiency (%)	90-92	85-97	78-86
Range of speeds (r/min)	12K-20K	4K-10K	More than 15K
Reliability	Good	Better	Good
Volume	Medium	Small	Small
Mass	Medium	Light	Light
Control Performance	Good	Good	Good
Manufacturing costs	Medium	High	Medium

The PMSM is a popular candidate because of its high power density, high efficiency and compact volume. But the disadvantage is the magnetic materials used in the PMSM are really expensive, and they need to be well maintained for the reason of magnet corrosion or demagnetization. The SRM is another promising candidate for EV applications, because of its simple structure, fault tolerant operation, and wide speed range at constant power. However, the disadvantages of the SRM are its high torque ripples and low efficiency [11, 15]. As a result of these researches, the induction motor is considered as the best candidate for the most of EVs applications [3, 5]. Intelligent, reliable and commercialized control systems of AC induction motors are being developed based on power electronic devices and digital signal processing (DSP) technology.

1.4 Research Objectives and Thesis Outline

Since an induction motor is a complicated nonlinear system, the electric rotor variables are not measurable directly, and the physical parameters of an induction motor are often imprecisely known. Meanwhile, the induction motor used in electric vehicle applications usually requires both fast transient responses and excellent steady state speed performance. All of these make the control of induction a challenging problem.

Lots of research has been done in the area of controlling an induction motor, some control methods result in an excellent steady state performance (e.g. Field Orientation Control (FOC)), others provide a great dynamic response (e.g. Direct Torque Control (DTC)), and there are some algorithms aiming at coupling the advantages from both side (e.g. stator flux orientated sensorless DTC). But no one has given a specific comparison among three of them. Thus an elaborate comparison is very necessary.

The main focus of this work is to design an induction motor control system using three algorithms mentioned above: FOC, DTC, and stator flux orientated sensorless DTC. The performances of different control algorithms will be analyzed, at the same time, these algorithms will be validated experimentally. Finally, the simulation results will be compared with experimental ones.

Thus, the scope of work of this project can be outlined by the following steps:

Step 1. Develop simulation models for each control algorithm.

Step 2. Compare simulation results for each control algorithm.

Step 3. Size the components for an induction motor control test bench and design peripheral circuits.

Step 4. Validate the effectiveness of the controller experimentally

Step 5. Compare simulation results with the experimental results.

This thesis is organized as follows:

The literature review for this work is summarized in Chapter 2. Chapter 3 presents the induction motor modeling basics, including the modeling tools and the modeling equations. The theory and implementation of filed orientation control for an induction motor will be introduced in Chapter 4, and in Chapter 5, the Direct Torque Control and Stator flux oriented sensorless DTC will be presented. Chapter 6 will focuses on the simulation results analysis, and in Chapter 7, the hardware setup and experimental results will be presented. The overall conclusions and future work are presented in Chapter 8.

CHAPTER II. LITERATURE REVIEW

2.1 Induction Motor Control Algorithms

The most commonly used control methods for AC induction motors are field orientation control, and direct torque control.

2.1.1 Field Oriented Control

The vector control techniques started developing around 1970 [16]. A few types of vector control, such as rotor flux oriented, stator flux oriented and mutual flux oriented are published one after another. No matter what kind of vector control, they are all subjected to imitate a separately excited DC motor, in which the electromagnetic torque and magnetic field can be controlled separately.

Field oriented control (FOC) has the capability of controlling both the field-producing and the torque-producing currents in a decoupled way [16]. For different applications, people might choose different flux orientation for some special demands. However, only the rotor flux oriented control achieves a complete decoupled system.

The field oriented control refers in particular to the rotor flux oriented type of vector control. Furthermore, the field oriented control can be classified into indirect or direct field oriented control, depending on how to obtain the rotor flux orientation.

The direct FOC obtains the orientation of the mutual flux by installing a hall-effect sensor inside the induction motor. However, using these type sensors is expensive and inconvenient, because special modifications need to be made in order to place the flux sensors. Furthermore, it is impossible to sense the rotor flux, so we have to sense the mutual flux directly and then calculate out the rotor flux information.

On the other hand, the indirect FOC is based on estimating the rotor flux orientation.

By using the signals from the motor terminals such as three phase currents and rotor rotating speed, the rotor flux orientation can be estimated using motor state equations. Indirect FOC does not have the problems that direct FOC does, which makes it popular in most applications.

2.1.2 Direct Torque Control

Direct torque control (DTC) was introduced in Japan by Takahashi and Nagochi [17] and also in Germany by Depenbrock [18]. This control algorithm does not follow the well developed DC motor control strategies. Instead of doing the coordinate transformations to decouple the electromagnetic torque and magnetic field, it employs a bang-bang control by using the hysteresis-controller. The bang-bang control works perfectly with the semiconductor inverter. As the name indicates, the most important feature of direct torque control is that it controls the electromagnetic torque and stator flux directly.

The typical DTC includes two hysteresis controllers [19]. Usually before implementing the hysteresis-controller, the actual stator flux is calculated from the stator voltages, and electromagnetic torque is calculated from the stator voltages and stator currents.

Therefore, the DTC control method strongly depends on the stator variables. As the stator voltage changes, the stator flux follows rapidly while the rotor flux changes slowly. This will modify the angle between stator and rotor fluxes and consequently the electromagnetic torque will be increased or decreased.

In the hysteresis-control section, a two-level stator flux hysteresis controller and a three-level torque hysteresis controller are commonly employed in the DTC scheme. One of the two flags will be generated from the stator flux hysteresis controller, when the actual stator flux is compared with its reference. On the other side, one of the three

flags will come out from the torque hysteresis controller. Furthermore, a sector number in which the stator flux vector lies need to be calculated out.

Using flux flag, torque flag, and flux sector number together as inputs, a voltage lookup table is then employed here. The appropriate voltage vector for the inverter is selected from the lookup table based on whether a need to increase or decrease the torque and stator flux. DTC attracts many researchers because of its fast torque response and simple control method [19, 20].

2.2 Comparison of Induction Motor Control Algorithms

An objective comparison between FOC and DTC is actually difficult to make since each author has his/her own specific demands and predilections. The most distinct differences can be given as: the orientation of FOC is usually on rotor flux while that of DTC is always on stator flux. Another difference is that two current controllers are necessary for FOC but which are replaced by a switching table in DTC.

The presence of a current controller could be an advantage of regulating the currents fluctuations. In practical operations, however, it is a limiting factor in terms of the transient performance. On the other hand, the two separate hysteresis controllers for flux and torque in DTC are able to immediately apply the maximum voltage to the motor which results in a better torque response.

Generally speaking, DTC provides a better dynamic torque response while FOC provides a better steady state behavior. But for vehicular applications, both steady state and dynamic performance are important to the system.

So it is obvious to imagine that if there is a control method which combines the advantages of FOC and DTC together, then both steady state and dynamic performance could be achieved. Actually, some research has been done in the field of

combining FOC and DTC to improve both the steady state as well as dynamic performance, [21-25].

One of the developed methods is stator flux orientated sensorless direct torque control. This control method is based on direct torque control, so the torque and flux responses can be guaranteed. At the same time the stator flux orientation technique is applied to predict the rotor speed. The flux orientation is a necessary part in FOC and because of this FOC achieves the decoupled currents and shows an excellent speed behavior. Thus, a DTC scheme with the flux orientation technique will surely provide a well regulated speed performance. In addition, the speed sensor can be eliminated from the system, since the rotor speed can be estimated instead of being measured. The absence of the speed sensor, either optical encoder or hall-effect speed sensor will definitely improve the ruggedness and reduces the cost of the entire system.

CHAPTER III. INDUCTION MOTOR MODELING

3.1 Induction Motor Basics

Three phase induction motors are rugged, cheap to produce and easy to maintain. They can run at a nearly constant speed from zero to full load. The design of an induction motor is relatively simple and consists of two main parts, a stationary stator and a rotating rotor. There are two main classes of the induction motor differing in the way their rotors are wound: the wound induction motor and the squirrel cage induction motor.

The motor discussed in this thesis is a three phase squirrel cage induction motor. The rotor of a squirrel cage induction motor consists of aluminum bars which are short circuited by connecting them to two end rings so that rotor generates the induction current and magnetic field by itself. This makes the AC induction motor a robust, rugged and inexpensive candidate for motor drive systems [26].

The structure of a squirrel cage induction motor is shown in Figure 9. In an induction motor, the alternating currents feed from three phase terminals and flow through the stator windings, producing a rotating stator flux in the motor [26]. The rotating speed of this magnetic field is defined as synchronous speed, and related to the number of poles of the induction motor and the frequency of power source.

$$n_{sync} = \frac{120\, f_e}{P} \quad rpm \tag{3.1}$$

where f_e is the power source frequency, P is the number of poles and n_{sync} is the synchronous speed in revolutions per minute.

The rotating magnetic field from the stator will induce a voltage in the rotor bars, since the rotor bars are short-circuited, a large circulating current will be generated in the rotor bars. This induced rotor current will then interact with the rotating magnetic

field. Because of Lorentz's law, a tangential electromagnetic force will be generated on the rotor bars, and the sum of forces on each rotor bar produces a torque that eventually drives the rotor in the direction of the rotating field.

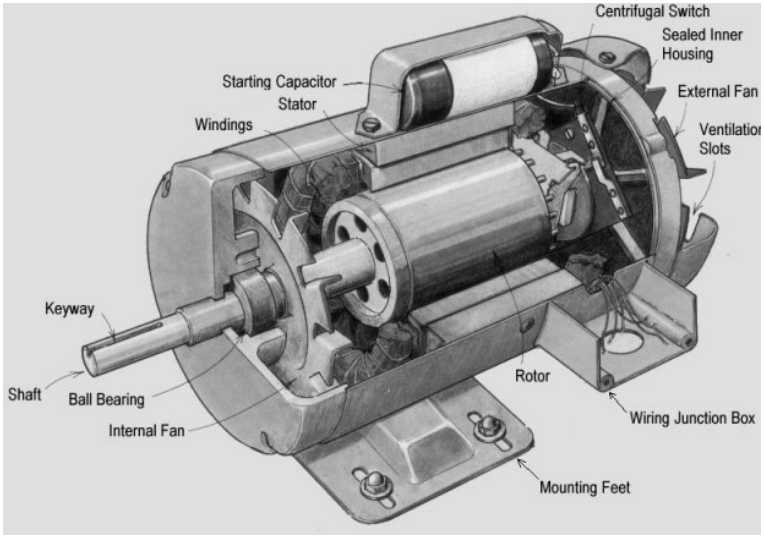

Figure 9: Squirrel cage induction motor cross section [14]

When the rotating magnetic field is first generated, the rotor is still in its rest condition. However, the rotor will accelerate rapidly in order to keep up with the rotating stator flux. As the rotor speed increases, the rotor bars are not cut as much by the rotating field, so the voltage in the rotor bars decreases. If the rotor speed equals to the flux speed, the rotor bars will no longer be cut by the field and the rotor will start to slow down [26]. This is why induction motors are also called asynchronous motors because the rotor speed will never equal the synchronous speed. The difference between the stator and rotor speed is defined as the slip speed:

$$n_{slip} = n_{sync} - n_m \tag{3.2}$$

where n_{slip} is the slip speed

$n_{sync}$is the speed of the rotating magnetic field

n_m is the mechanical shaft speed of the motor

Also, a slip ratio can be defined as:

$$s = \frac{n_{sync} - n_m}{n_{sync}} \tag{3.3}$$

Notice that, if the rotor runs at synchronous speed

$$s = 0 \tag{3.4}$$

if the rotor stops moving

$$s = 1 \tag{3.5}$$

3.2 Space Vectors

By using space vectors in the induction motor modeling, all the complex state variables can be efficiently defined [27]. Variables such as the three phase voltages, currents and fluxes of induction motors can be analyzed and described easily and conveniently.

The three phase axes are defined by the vectors: e^{j0°, e^{j120° and e^{j240°. The stator windings and stator current space vector in the complex plane are shown in below.

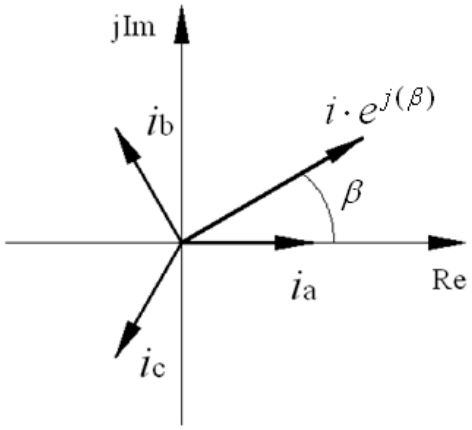

Figure 10: Current space vectors

The space vector of the stator current i_s can be described by:

$$i_s = i_{as} \cdot e^{j0^\circ} + i_{bs} \cdot e^{j120^\circ} + i_{cs} \cdot e^{j240^\circ} \tag{3.6}$$

where subscript s refers to the stator of the induction motor, a, b, and c are the three phase axes.

Furthermore, the rotor current can be described by:

$$i_r = i_{ar} \cdot e^{j0^\circ} + i_{br} \cdot e^{j120^\circ} + i_{cr} \cdot e^{j240^\circ} \tag{3.7}$$

where subscript r refers to the rotor of the induction motor.

3.3 The Coordinate Transformation of Space Vectors

The modeling, analysis and control design of induction can be significantly simplified by using coordinate transformations. A three-phase variable can be transferred into a two-phase variables [28]; also a stationary variable can be transferred into a rotational one [29]. This transformation usually includes the following two steps:

- The Clarke transformation
- The Park transformation

3.3.1 Clarke Transformation

The Clarke transformation transfers a three-phase system into a two-phase system. Take the currents, for example:

$$\begin{pmatrix} i_\alpha \\ i_\beta \end{pmatrix} = \begin{pmatrix} \frac{2}{3} & -\frac{1}{3} & -\frac{1}{3} \\ 0 & \frac{\sqrt{3}}{3} & -\frac{\sqrt{3}}{3} \end{pmatrix} \cdot \begin{pmatrix} i_a \\ i_b \\ i_c \end{pmatrix} \tag{3.8}$$

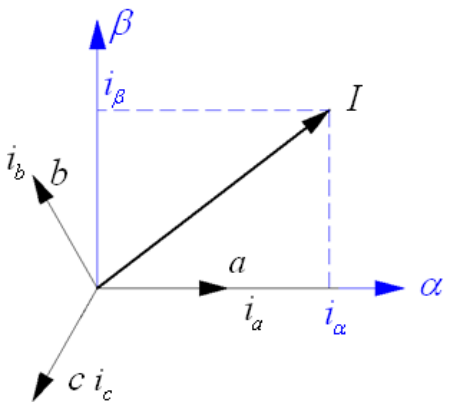

Figure 11: Clarke transformation of three-phase currents

In this thesis, $(a,b,c) \Rightarrow (\alpha,\beta)$ is used to represent the Clarke transformation.

3.3.2 Park Transformation

The Park transformation transfers a stationary system into a rotational system:

$$\begin{pmatrix} i_d \\ i_q \end{pmatrix} = \begin{pmatrix} \cos\theta & \sin\theta \\ -\sin\theta & \cos\theta \end{pmatrix} \cdot \begin{pmatrix} i_\alpha \\ i_\beta \end{pmatrix} \tag{3.9}$$

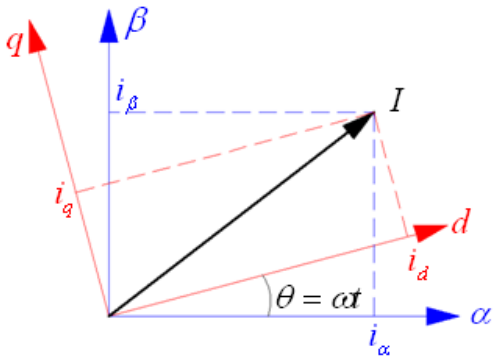

Figure 12: Park transformation of two-phase currents

Here $(\alpha, \beta) \Rightarrow (d, q)$ is used to represent the Park transformation.

3.4 Modeling Equations

The induction motor modeling usually contains three parts: flux equations, voltage equations and torque equations [27].

3.4.1 Flux Equations

There are three kinds of fluxes: stator flux, rotor flux and mutual flux. The stator flux and rotor flux vectors can be expressed in terms of stator current i_s and rotor current i_r, given below:

$$\Psi_s = L_s I_s + L_m I_r \tag{3.10}$$

$$\Psi_r = L_r I_r + L_m I_s \tag{3.11}$$

where L_s and L_r are the stator inductance and the rotor inductance, respectively; L_m is the mutual inductance between the stator and rotor windings.

3.4.2 Voltage Equations

As we mentioned above, the voltage equations of induction motors can be described

in different coordinate frames. Three kinds of coordinate frames are commonly used to describe the induction motors [27]. They are:

- Stationary frame;
- Synchronous rotating frame;
- Field orientation synchronous frame.

3.4.2.1 Voltage Equations in Stationary Frame

The induction motor usually has three sets of stator windings, and the rotor can be considered as three sets of windings as well [27]. Both stator and rotor can be represented by inductance and resistance in an equivalent-circuit. Using the Clarke transformation, the three-phase induction motor model can be expressed as an equivalent two-phase model [27]. The equivalent circuits in the stationary frame of the induction motor are shown in Figure 13 and 14:

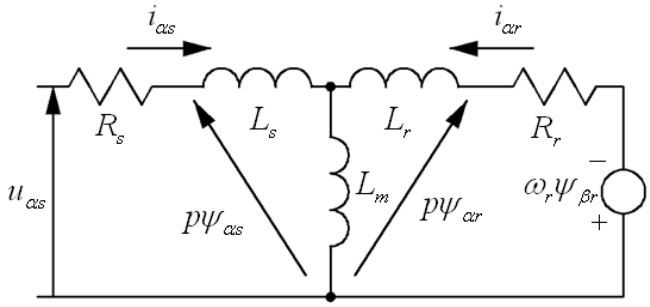

Figure 13: Alpha component of the induction motor equivalent-circuit

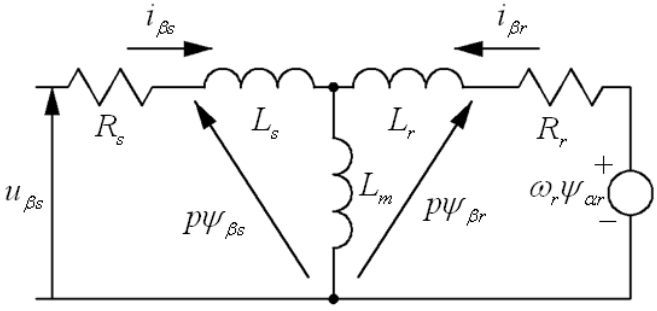

Figure 14: Beta component of the induction motor equivalent-circuit

Based on the Kirchhoff's voltage law (KVL), the stator and rotor voltage equations can be expressed as:

$$u_{\alpha s} = i_{\alpha s} R_s + p\psi_{\alpha s} \tag{3.12}$$

$$u_{\beta s} = i_{\beta s} R_s + p\psi_{\beta s} \tag{3.13}$$

$$0 = i_{\alpha r} R_r + p\psi_{\alpha r} + \omega_r \psi_{\beta r} \tag{3.14}$$

$$0 = i_{\beta r} R_r + p\psi_{\beta r} - \omega_r \psi_{\alpha r} \tag{3.15}$$

where $\omega_r \psi_{\beta r}$ and $\omega_r \psi_{\alpha r}$ are rotating velocity emf and p is the differential operator.

Substituting eq. 3.10 and 3.11 into eq. 3.12 and eq. 3.13, the stator voltage equations can be rewritten:

$$u_{\alpha s} = (R_s + L_s p) i_{\alpha s} + L_m p i_{\alpha r} \tag{3.16}$$

$$u_{\beta s} = (R_s + L_s p) i_{\beta s} + L_m p i_{\beta r} \tag{3.17}$$

Also, the rotor voltage equations can be rewritten as:

$$0 = L_m p i_{\alpha s} + (R_r + i_r p) i_{\alpha r} + \omega_r L_m i_{\beta s} + \omega_r L_r i_{\beta r} \tag{3.18}$$

$$0 = L_m p i_{\beta s} + (R_r + i_r p) i_{\beta r} - \omega_r L_m i_{\alpha s} - \omega_r L_r i_{\alpha r} \tag{3.19}$$

The relationship of voltages and currents can be given in matrix form from the four voltage equations:

$$\begin{pmatrix} u_{\alpha s} \\ u_{\beta s} \\ 0 \\ 0 \end{pmatrix} = \begin{pmatrix} (R_s + L_s p) & 0 & L_m p & 0 \\ 0 & (R_s + L_s p) & 0 & L_m p \\ L_m p & \omega_r L_m & (R_r + L_r p) & L_r \omega_r \\ -L_m \omega_r & L_m p & -L_r \omega_r & (R_r + L_r p) \end{pmatrix} \cdot \begin{pmatrix} i_{\alpha s} \\ i_{\beta s} \\ i_{\alpha r} \\ i_{\beta r} \end{pmatrix} \tag{3.20}$$

where ω_r is rotor speed.

3.4.2.2 Voltage Equations in Synchronous Rotating Frame

This is a rotary frame and the rotating speed is ω_e. Using the Park transformation, eq. 3.12, and 3.13 can be expressed in the d-q synchronous rotating reference frame, so the stator voltage equations can be rewritten as:

$$u_{ds} = i_{ds} R_s + p\psi_{ds} - \omega_e \psi_{qs} \tag{3.21}$$

$$u_{qs} = i_{qs}R_s + p\psi_{qs} + \omega_e\psi_{ds} \tag{3.22}$$

The last terms in eq. 3.21 and eq. 3.22 can be defined as speed emf as they are directly related with the synchronous speed of the motor. When $\omega_e = 0$, these equations turn back to stationary forms.

Similarly, the rotor voltage equations can be derived from eq. 3.14 and eq. 3.15. At this time, the rotor speed is ω_r, and since the d-q axes are fixed with the rotor, the relative speed with respect of synchronously rotating frame is $\omega_e - \omega_r$. Therefore, in the synchronous rotating frame, the rotor voltage equations should be rewritten as:

$$0 = i_{dr}R_r + p\psi_{dr} + (\omega_r - \omega_e)\psi_{qr} \tag{3.23}$$

$$0 = i_{qr}R_r + p\psi_{qr} - (\omega_r - \omega_e)\psi_{dr} \tag{3.24}$$

The stator voltage equations can be rewritten as:

$$u_{ds} = i_{ds}(R_s + L_s p) - L_s\omega_e i_{qs} - L_m\omega_e i_{dr} + L_m p i_{qr} \tag{3.25}$$

$$u_{qs} = i_{qs}(R_s + L_s p) + L_s\omega_e i_{ds} + L_m\omega_e i_{dr} + L_m p i_{qr} \tag{3.26}$$

The rotor voltage equations can be rewritten as:

$$0 = L_m p i_{ds} - (\omega_e - \omega_r)L_m i_{qs} + (R_r + L_r p)i_{dr} - L_r(\omega_e - \omega_r)i_{qr} \tag{3.27}$$

$$0 = L_m p i_{qs} + (\omega_e - \omega_r)L_m i_{ds} + (R_r + L_r p)i_{qr} + L_r(\omega_e - \omega_r)i_{dr} \tag{3.28}$$

Equations 3.25 – 3.28 also can be expressed in a matrix form as:

$$\begin{pmatrix} u_{ds} \\ u_{qs} \\ 0 \\ 0 \end{pmatrix} = \begin{pmatrix} (R_s + L_s p) & -L_s\omega_e & L_m p & -L_m\omega_e \\ L_s\omega_e & (R_s + L_s p) & L_m\omega_e & L_m p \\ L_m p & -L_m(\omega_e - \omega_r) & (R_r + L_r p) & -L_r(\omega_e - \omega_r) \\ L_m(\omega_e - \omega_r) & L_m p & L_r(\omega_e - \omega_r) & (R_r + L_r p) \end{pmatrix} \cdot \begin{pmatrix} i_{ds} \\ i_{qs} \\ i_{dr} \\ i_{qr} \end{pmatrix} \tag{3.29}$$

3.4.3 Torque Equations

A torque is produced as a result of the interaction of stator magnetic field and rotor

magnetic field [30], so one can have:

$$T_e = K_0 B_r \times B_s \tag{3.30}$$

where T_e is the induced torque and B_r and B_s are the magnetic flux densities of the rotor and the stator respectively.

Also, the electromagnetic torque is produced by the interaction of current and magnetic field. Using two current quantities (stator current and rotor current) and three fluxes (stator flux, mutual flux and rotor flux), the torque can be expressed in six different forms [31]:

$$T_e = K_1 \Psi_s \times I_r \tag{3.31}$$

$$T_e = K_2 \Psi_m \times I_r \tag{3.32}$$

$$T_e = K_3 \Psi_r \times I_r \tag{3.33}$$

$$T_e = K_4 \Psi_s \times I_s \tag{3.34}$$

$$T_e = K_5 \Psi_m \times I_s \tag{3.35}$$

$$T_e = K_6 \Psi_r \times I_s \tag{3.36}$$

where $K_1 \sim K_6$ are the torque coefficients. In fact, these six expressions are all identical.

Also, the system motion equation is given by:

$$T_e = T_L + \frac{J}{n_p} \cdot \frac{d\omega}{dt} \tag{3.37}$$

where T_L is the load torque, ω is the rotor rotating speed, and n_p is the poles numbers, and J is rotor's moment of inertia.

3.5 Inverter Control and Pulse Width Modulation Technology

3.5.1 Inverter Control

The induction motor can be connected directly to a standard fixed frequency, fixed voltage three phase power source. Under these conditions, the motor speed and slip will only be determined by the load torque. With no load, the slip is small so the rotor speed is close to synchronous speed. Using a variable frequency inverter in the induction motor driving system, both the magnitude and frequency of the voltage inputs can be adjusted based on certain control method.

A three phase inverter has three sets of power switches, and various supporting components such as capacitors to smooth switching voltages. Two switches account for one phase of the motor and appear in a leg of the inverter. By turning on and off the switches, the current flow into the motor will be generated and controlled. However, two switches in a leg are never turned on at the same time; otherwise this leg would be short circuited. Thus, eight combinations of switching state exist in a three phase inverter. In electromechanical systems, the losses in the power switches also become a concern, the switching frequency is typically controlled from 10 KHz to 20 KHz so switching losses can be minimized. [32-34]

3.5.2 Pulse Width Modulation (PWM) Technology

The average value of voltage fed to the load could be controlled by turning the switch between on and off at a very fast pace. The longer the switch is on as opposed to off, the higher the average value of the voltage output [35].

The main advantage of PWM technique is that power loss in the switching devices is very low. By adjusting the pulse width, the voltage output can be efficiently controlled [35].

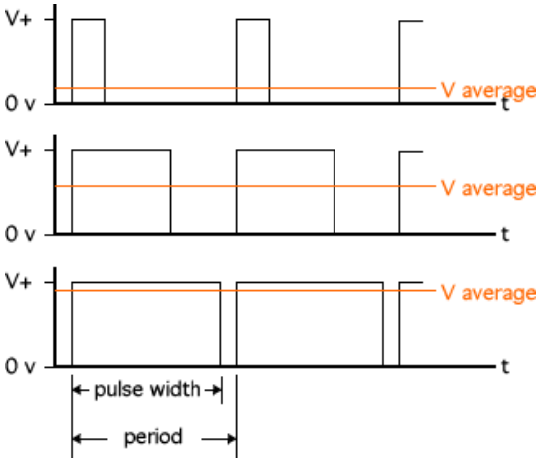

Figure 15: PWM techniques for time invariant signals [36]

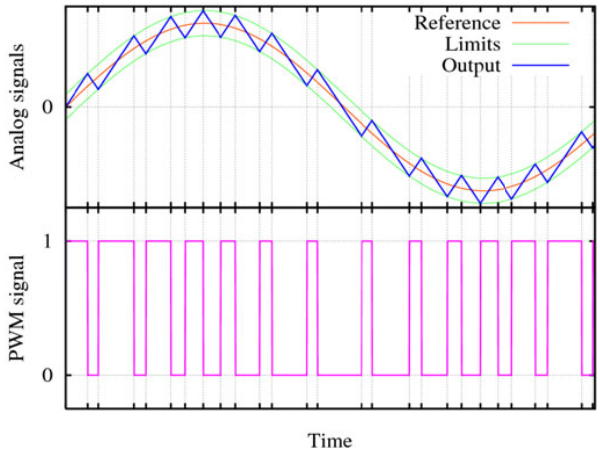

Figure 16: PWM techniques for time variant signals [36]

3.5.3 Space Vector Pulse Width Modulation (SVPWM) Technology

Space vector modulation is an advanced technique of PWM. It is commonly used to generate alternating currents and voltage for a three phase device, such as an induction motor.

The circuit model of a typical three-phase voltage source PWM inverter is shown in Figure 17. S_1 to S_6 are the six power switches. When an upper transistor is switched on, the corresponding lower transistor must be switched off; otherwise the DC power will be short-circuited. Therefore, the on and off states of the upper transistors S_1, S_3 and S_5 can be used to determine the output voltage.

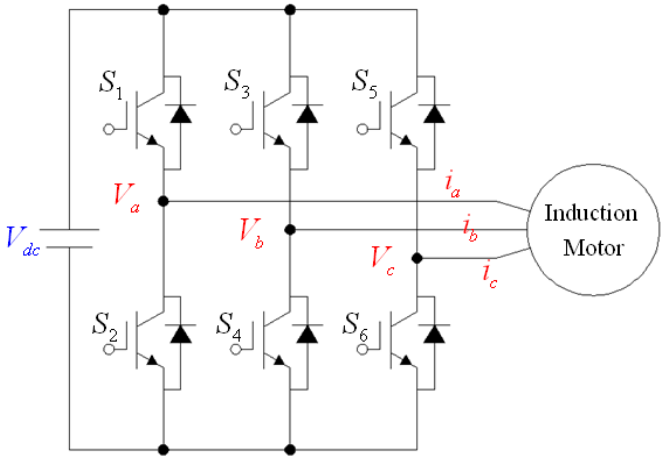

Figure 17: Three-phase voltage source inverter

The six transistors in the inverter can form 8 switch variables, 6 of them are nonzero vectors and 2 of them are zero vectors [37].

The relationship between the switching variable vector $[S_1, S_3, S_5]^T$ and the phase voltage $[V_{an}\ V_{bn}\ V_{cn}]^{T,}$ and the line to line voltage $[V_{ab}\ V_{bc}\ V_{ca}]^T$ can be expressed below:

$$\begin{pmatrix} V_{an} \\ V_{bn} \\ V_{cn} \end{pmatrix} = \frac{V_{dc}}{3} \begin{pmatrix} 2 & -1 & -1 \\ -1 & 2 & -1 \\ -1 & -1 & 2 \end{pmatrix} \begin{pmatrix} S_1 \\ S_3 \\ S_5 \end{pmatrix} \tag{2.1}$$

$$\begin{pmatrix} V_{ab} \\ V_{bc} \\ V_{ca} \end{pmatrix} = V_{dc} \begin{pmatrix} 1 & -1 & 0 \\ 0 & 1 & -1 \\ -1 & 0 & 1 \end{pmatrix} \begin{pmatrix} S_1 \\ S_3 \\ S_5 \end{pmatrix} \tag{2.2}$$

According to eq. 2.1 and eq. 2.2, the eight voltage vectors, switching vectors and the output line to neutral voltage can be summarized in the given table:

Table 2: Voltage vectors table [38]

Voltage vectors	Switching vectors			Line to neutral voltage (V_{dc})		
	S_1	**S_2**	**S_3**	V_{an}	V_{bn}	V_{cn}
V0	0	0	0	0	0	0
V1	1	0	0	2/3	-1/3	-1/3
V2	1	1	0	1/3	1/3	-2/3
V3	0	1	0	-1/3	2/3	-1/3
V4	0	1	1	-2/3	1/3	1/3
V5	0	0	1	-1/3	-1/3	2/3
V6	1	0	1	1/3	-2/3	1/3
V7	1	1	1	0	0	0

Also, these eight vectors could be plotted out in the Alfa-beta plane as shown below:

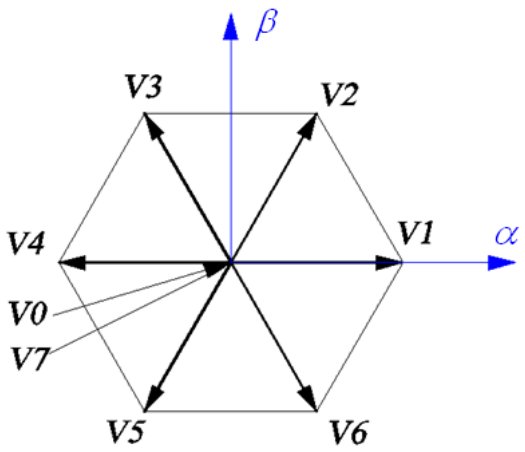

Figure 18: Voltage source inverter output vectors in the Alfa-beta plane [39]

The SVPWM output voltage waveforms are shown below, the first one is a saddle-shaped wave which represents the phase voltage, and the second one is the line to line output voltage.

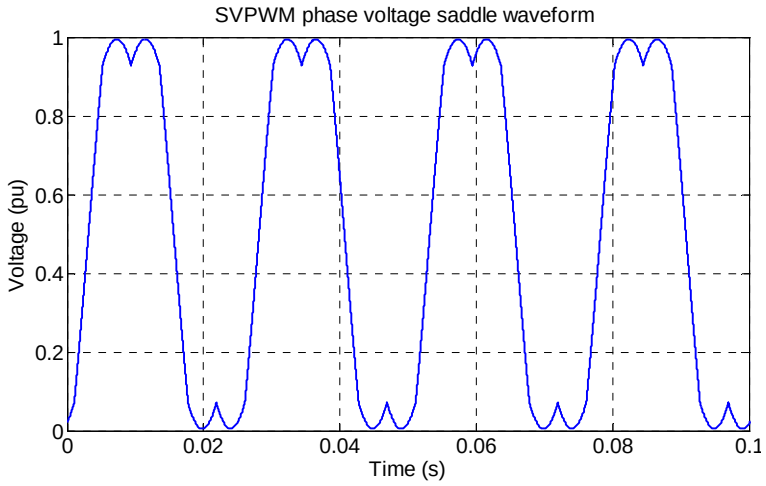

Figure 19: Phase voltage of SVPWM

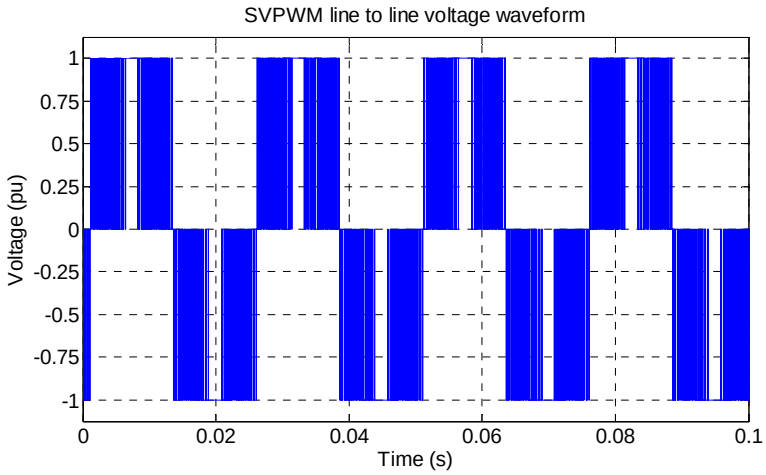

Figure 20: Line to line voltage of SVPWM

CHAPTER IV. THEORY OF FIELD ORIENTATION CONTROL

4.1 Philosophy of Field Orientation Control

Field orientation control is introduced by Hasse and Blaschke [16], and is a milestone in AC motor control field. It is also commonly known as vector control because it controls both the magnitude and direction of the variables. The distinguishing characteristic of field orientation control is to decouple the torque and flux. This method imitates the separately-excited DC motor which operates with separated torque and flux. Since the high order and nonlinear system nature make AC induction motors hard to control precisely, following this well developed DC motor control technique became a popular trend.

In order to describe the basic concept of field orientation control, we need to finish the third coordinate transformation: from synchronous rotating frame to rotor flux oriented reference frame [27].

This transformation is done to fix the d-axis of the synchronous rotating frame with the rotor flux direction of AC induction motor. Since the d-axis is aligned with the rotor flux direction, the flux d and q components can be rewritten as:

$$\psi_{dr} = \psi_r = L_r i_{dr} + L_m i_{ds} \tag{4.1}$$

$$\psi_{qr} = 0 = L_r i_{qr} + L_m i_{qs} \tag{4.2}$$

Substituting eq. 4.1 and 4.2 into eq. 3.27 and eq. 3.28 to simplify the rotor voltage equations, one can have:

$$0 = L_m p i_{ds} + (R_r + L_r p) i_{dr} \tag{4.3}$$

$$0 = (\omega_e - \omega_r) L_m i_{ds} + (\omega_e - \omega_r) L_r i_{dr} + R_r i_{qr} \tag{4.4}$$

Combining the stator eq. 3.25 and eq.3.26 with eq. 4.3 and 4.4, the rotor flux oriented

voltage equations can be rewritten in matrix form as:

$$\begin{pmatrix} u_{ds} \\ u_{qs} \\ 0 \\ 0 \end{pmatrix} = \begin{pmatrix} (R_s + L_s p) & -L_s\omega_e & L_m p & -L_m\omega_e \\ L_s\omega_e & (R_s + L_s p) & L_m\omega_e & L_m p \\ L_m p & 0 & (R_r + L_r p) & 0 \\ L_m(\omega_e - \omega_r) & 0 & L_r(\omega_e - \omega_r) & R_r \end{pmatrix} \cdot \begin{pmatrix} i_{ds} \\ i_{qs} \\ i_{dr} \\ i_{qr} \end{pmatrix} \quad (4.5)$$

In the matrix equation, the difference between the synchronous speed ω_e and rotor speed ω_r is the motor slip speed ω_{sl}.

$$\omega_{sl} = \omega_e - \omega_r \quad (4.6)$$

From the torque equation $T_e = K_6 \psi_r \times I_s$, one can have:

$$T_e = K_6(i_{qs}\psi_{dr} - i_{ds}\psi_{qr}) \quad (4.7)$$

Substituting the rotor flux eq. 4.2 $\psi_{qr} = 0$ into eq. 4.7, one has:

$$T_e = K_6 \cdot i_{qs}\psi_{dr} \quad (4.8)$$

Eq. 4.8 shows another important feature: when the flux level ψ_{dr} is a constant, the electromagnetic torque is determined by i_{qs}, which is completely decoupled form i_{ds}.

From eq. 4.1 and eq. 4.2, one can have:

$$i_{qr} = \frac{-L_m i_{qs}}{L_r} \quad (4.9)$$

$$i_{dr} = \frac{\psi_{dr} - L_m i_{ds}}{L_r} \quad (4.10)$$

From the rotor voltage equation 4.3, and flux eq. 4.2 one can have:

$$0 = R_r i_{dr} + p\psi_{dr} \quad (4.11)$$

Substituting eq. 4.10 into eq. 4.11, one can have:

$$0 = R_r\left(\frac{\psi_{dr} - L_m i_{ds}}{L_r}\right) + p\psi_{dr} \quad (4.12)$$

$$(1 + T_r p)\psi_{dr} = L_m i_{ds} \quad (4.13)$$

Consider eq. 4.13 as a transfer function G(p), and substitute it into eq. 4.8 $T_e = K_6 \cdot i_{qs} \psi_{dr}$ one can finally have the torque equation as:

$$T_e = K_6 \cdot i_{qs} \cdot \frac{L_m i_{ds}}{(1 + T_r p)} \tag{4.14}$$

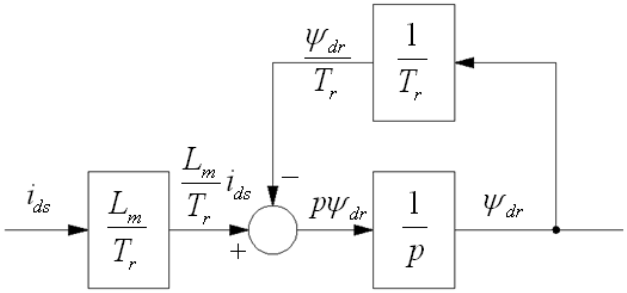

Figure 21: The transfer function G(p)

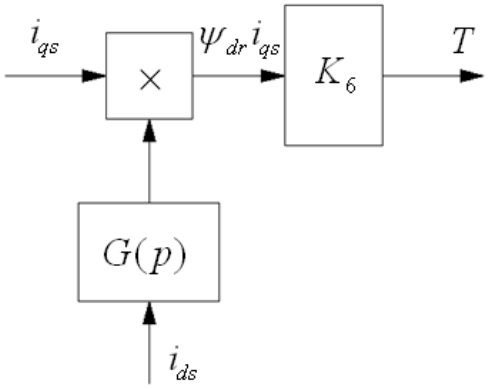

Figure 22: The electromagnetic torque is directly controlled by two decoupled currents

In field orientation control, there are two kinds of coordinate transformations: three phase to two phase (Clarke transformation), and stationary to rotation (Park transformation). To accomplish the rotating transformation, the flux angle θ_e must be known precisely [27].

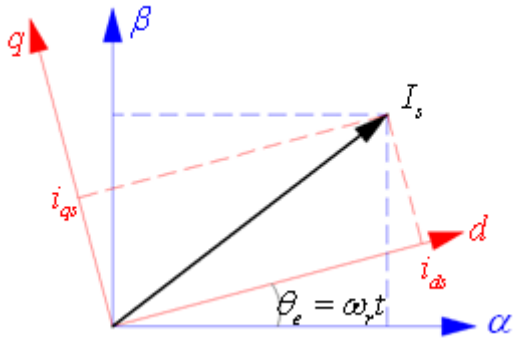

Figure 23: The rotating angle between the stationary and rotational frames

There are two basic ways to obtain the angle information: one is direct measurement, another is indirect estimation. Therefore, we end up having two types of field orientation control: Direct Field Orientation Control (DFOC) and Indirect Field Orientation Control (IFOC) [27].

4.2 Direct Field Orientation Control (DFOC)

Direct field orientation control was first proposed by F. Blaschke [16]. In order to capture the flux information of the motor, flux sensors, such as hall flux sensors, can be used to measure the mutual magnetic fields Ψ_m. Mount the flux sensors inside of the motor; and thus, two components $\Psi_{m\alpha}$ and $\Psi_{m\beta}$ of the mutual magnetic fields can be detected.

Based on the motor flux equations:

$$\Psi_r = L_r I_r + L_m I_s \tag{4.15}$$

$$\Psi_m = L_m I_r + L_m I_s \tag{4.16}$$

The rotor flux can be expressed by eliminating rotor current Ir:

$$\Psi_r = \frac{L_r}{L_m}\Psi_m - (L_r - L_m) I_s \tag{4.17}$$

Use the measured mutual flux component $\Psi_{m\alpha}$ and $\Psi_{m\beta}$ the rotor components in

two axes can be obtained as:

$$\psi_{\alpha r} = \frac{L_r}{L_m}\psi_{\alpha m} - (L_r - L_m)i_{\alpha s} \tag{4.18}$$

$$\psi_{\beta r} = \frac{L_r}{L_m}\psi_{\beta m} - (L_r - L_m)i_{\beta s} \tag{4.19}$$

The rotor flux magnitude and angle can be further expressed as:

$$\psi_r = \sqrt{\psi_{\alpha r}{}^2 + \psi_{\beta r}{}^2} \tag{4.20}$$

$$\cos\theta_e = \frac{\psi_{\alpha r}}{\sqrt{\psi_{\alpha r}{}^2 + \psi_{\beta r}{}^2}} \tag{4.21}$$

Figure 24 shows the calculation process of rotor flux by using hall sensors:

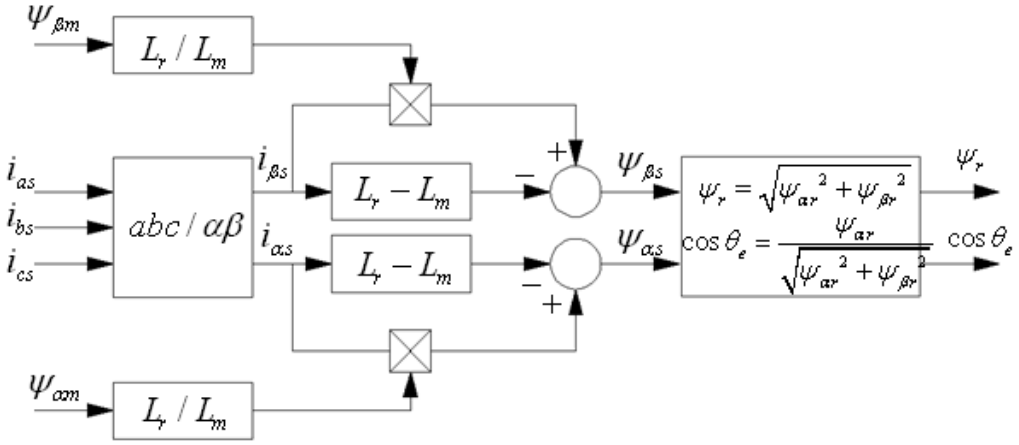

Figure 24: The calculation of flux magnitude and angle [40]

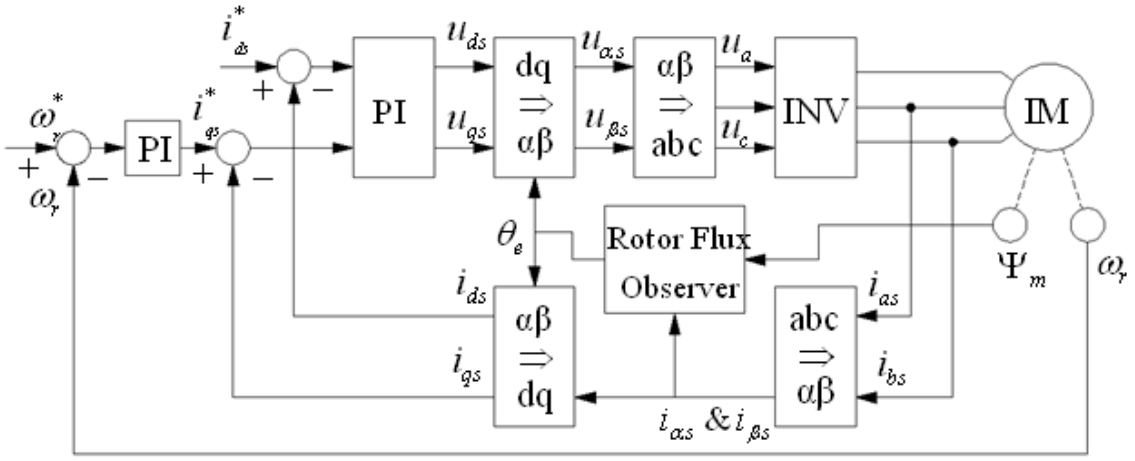

Figure 25: DFOC system diagram

It is not convenient to install a hall affect flux sensor inside the motor, and it is not

practical for most industrial applications. Also, it will definitely decrease the reliability of the drive system [41]. A preferable approach is to use the flux observer to estimate or calculate the rotor flux to implement the field orientation control.

4.3 Indirect Field Orientation Control (IFOC)

Indirect field orientation control (IFOC) was proposed by K. Hasse [42]. Instead of using the flux sensors, IFOC calculates the rotor flux angle from some intermediate variables, such as the slip speed ω_{sl} and rotor speed ω_r :

From the eq. 4.6 $\omega_{sl} = \omega_e - \omega_r$, one can have:

$$\theta_e = \int \omega_e dt = \int (\omega_{sl} + \omega_r) dt \tag{4.22}$$

Since Ψ_r is fixed with respect to the d-axis of rotating frame, the flux components in q axis can be expressed as follows:

$$0 = R_r i_{qr} + (\omega_e - \omega_r)\psi_{dr} \tag{4.23}$$

Substitute eq. 4.9 into eq. 4.23:

$$0 = R_r \left(\frac{-L_m i_{qs}}{L_r}\right) + (\omega_e - \omega_r)\psi_{dr} \tag{4.24}$$

And finally, we end up having:

$$\omega_{sl} = (\omega_e - \omega_r) = \frac{L_m i_{sq}}{T_r \psi_{dr}} \tag{4.25}$$

From eq. 4.13 $(1 + T_r p)\psi_{dr} = L_m i_{ds}$, the slip speed can be further expressed as:

$$\omega_{sl} = \frac{(1 + T_r p)}{T_r} \frac{i_{qs}}{i_{ds}} \tag{4.26}$$

On the other hand, the rotor speed ω_r is measured from a speed sensor attached on the motor shaft, by combining these two speeds, we can calculate out the flux angle from eq. 4.22. This is the basic concept of IFOC.

In a field orientation control system, the motor currents are measured from the any

two of the three terminals, transformed by two coordinate conversions, and regulated by two separated PI current controllers.

Figure 26 shows the indirect field orientation control system based on the calculation of slip speed.

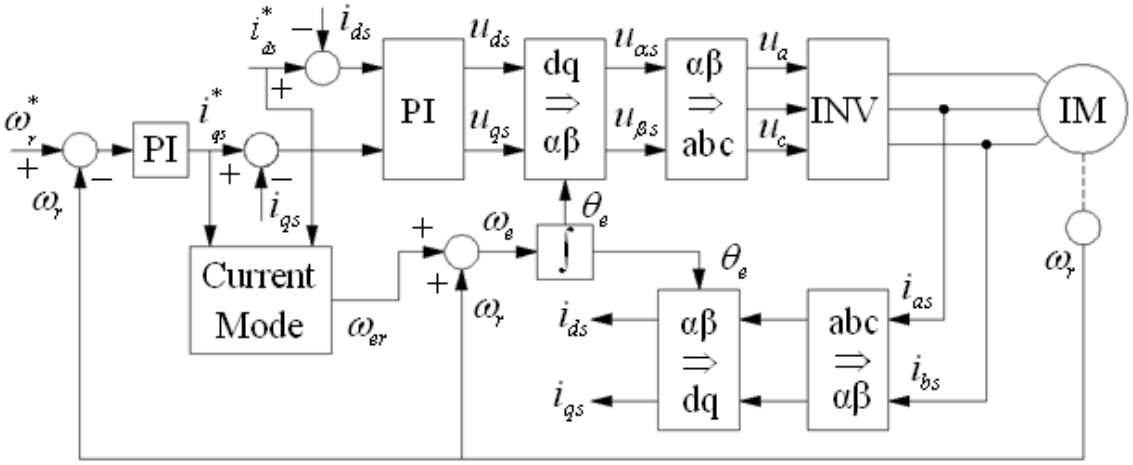

Figure 26: The system diagram of IFOC

IFOC is very sensitive to motor parameters (rotor time constant T_r) [43]. Therefore, T_r must be precisely known in order to realize decoupled control of torque and flux. When T_r is not set correctly, the controller is said to be detuned, and the performance will be degraded. Hence rotor time constant estimations or online adaptive identifications have been studied extensively in IFOC [43-47]. Significant efforts have been made towards an efficient and accurate identification of rotor time constant and to overcome the detuning effect [48-50].

4.4 Implement of IFOC

First of all, three phase stator currents i_a, i_b, and i_c are transformed into two phase currents i_α and i_β using Clarke transformation.

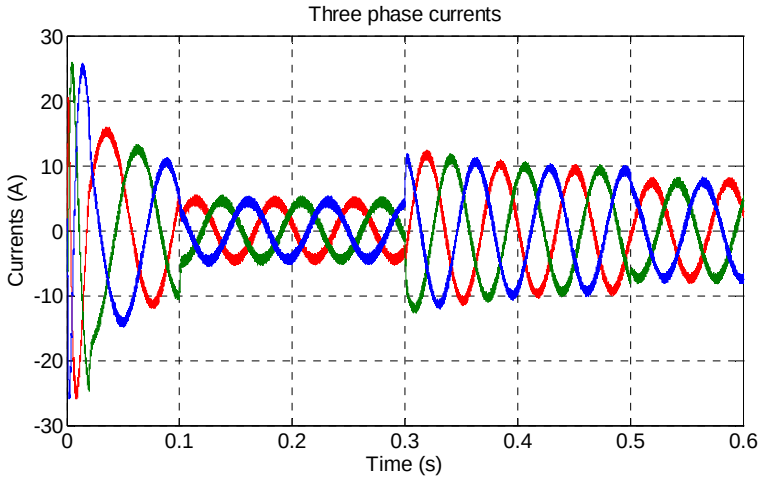

Figure 27: Three phase stator currents in FOC

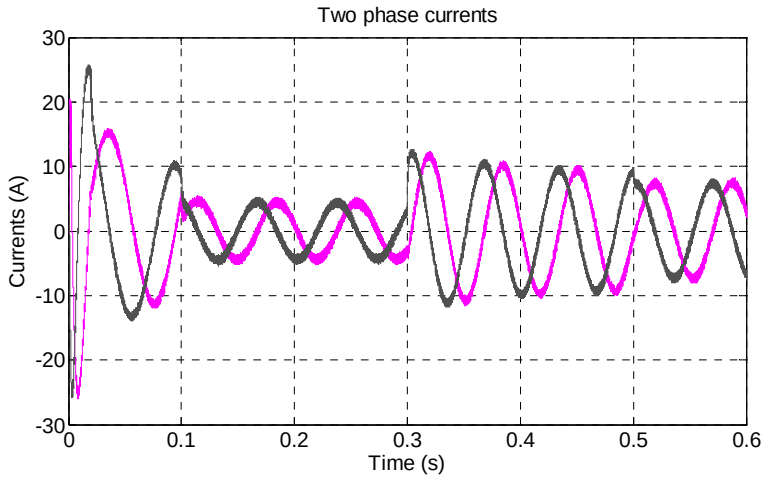

Figure 28: Two phase currents after Clarke transformation in FOC

Two phase currents are then being transferred into a synchronous rotating frame from the previous stationary frame. For FOC we discuss in this thesis, the d-axis in the synchronous frame is aligned with the rotor flux direction, so the complete decouple between two phase currents can be achieved. The decoupled currents are shown below: on the one hand, current I_{qs} is required for generating the electromagnetic torque, so it is proportional to the torque command. Current I_{ds} is responsible for generating the rotor flux in induction motor, so after a very short period time at the beginning, the current I_{ds} should remain as a constant. The FOC does not control the flux in the motor, so during the starting period, the rotor flux gradually increases from zero to the rated value, and then maintains around this value. This phenomenon is shown in Figure 31 below.

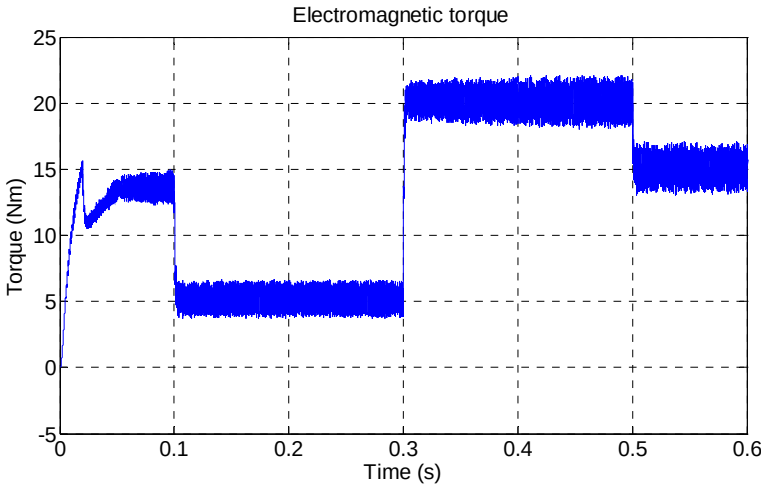

Figure 29: Torque response based on the requirement

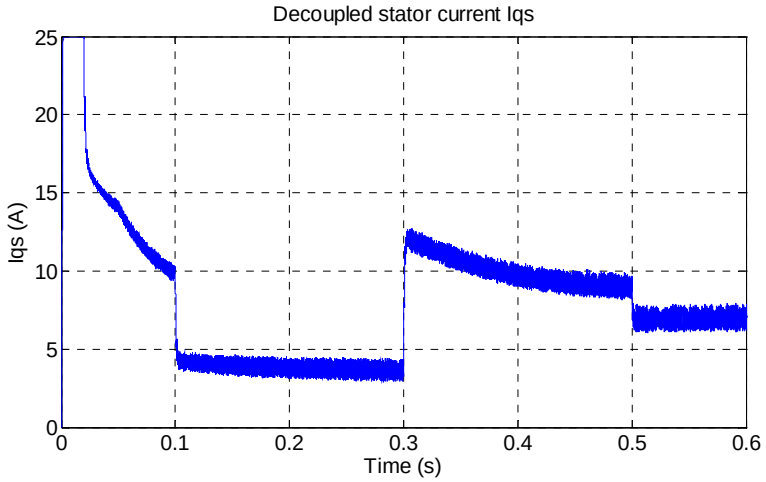

Figure 30: Decoupled current I_{qs} which is responsible for generating torque

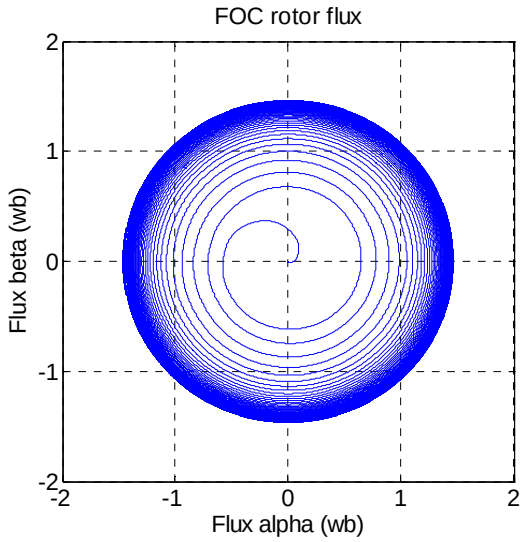

Figure 31: Rotor flux trajectory in FOC

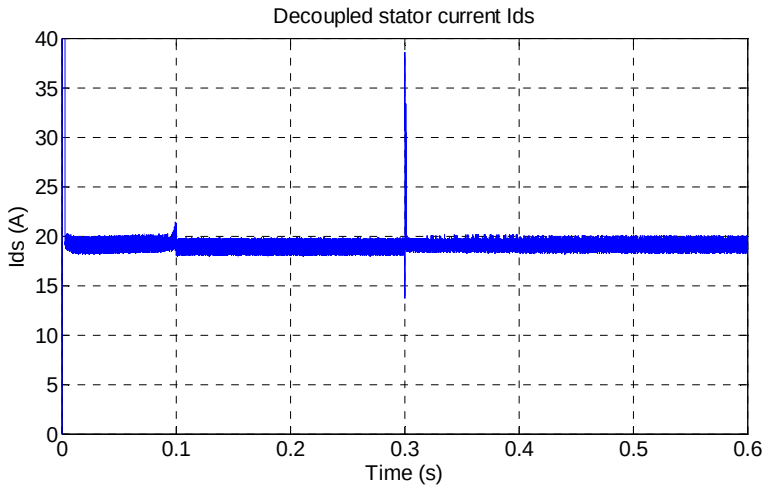

Figure 32: Decoupled current I_{ds} which is responsible for generating flux

4.5 FOC Summary

The main features of FOC are summarized as follows:

- The torque and flux control are decoupled;
- A modulator which converts the voltage command outputs of the current regulator into switching states of the inverter is needed in the system;
- Two coordinate frame transformations are required;
- No direct torque feedback control occurs; torque control is indirect.

But for DFOC and IFOC, they have some different features:

◇ DFOC:

- The information of the rotor, the stator or the mutual flux is required. Usually, it is measured by hall-affect sensors inside the motor;
- Closed loop control of flux amplitude is possible, but might not be required.

◇ IFOC:

- The information of rotor, stator or mutual flux is not necessary;
- The actual rotor flux amplitude is controlled by the reference value;
- The rotor flux position (rotor flux angle) needs to be estimated.

CHAPTER V. THEORY OF CONVENTIONAL DIRECT TORQUE CONTROL AND STATOR FLUX ORIENTATED SENSORLESS DIRECT TORQUE CONTROL

5.1 Control Strategy of Conventional Direct Torque Control

Direct torque control of the AC induction motor is relatively newer than field orientation control. This technique was first published in the mid-1980's, by Depenbrock and Takahashi [18, 17]. It is believed to have nearly comparable performance of field orientation control [51]. The distinguishing characteristic of the direct torque control is that torque and flux are controlled directly; but in field orientation control, the stator currents (both d and q axes) are controlled directly.

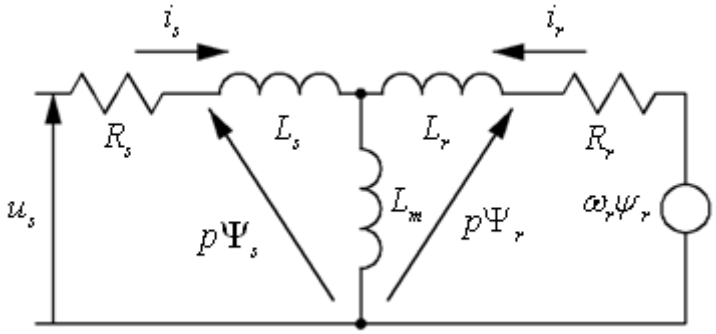

Figure 33: Equivalent- circuit of induction motor in the stationary frame

From the equivalent-circuit in the stationary frame of induction motor, one can have:

$$\frac{d\Psi_s}{dt} = u_s - R_s i_s \tag{5.1}$$

From the equation 6.1, if the voltage drop on the stator resistor is neglected, one can derive that the change of the stator flux vector over a given time period is equal to the voltage vector applied on stator:

$$\Psi_s(t) = \int_0^t u_s dt \tag{5.2}$$

On the other hand, when the AC induction motor is working, it could be noticed that the stator flux can be changed rapidly by applying the voltage vectors on the stator

while the rotor flux will not respond as quickly as enough [52]. So the position and the angle between the stator and rotor flux will be changed immediately.

Since we have the torque equation:

$$T_e = K_0 \left|\Psi_s\right| \cdot \left|\Psi_r\right| \sin\theta \qquad (5.3)$$

Assume that the rotor flux moves as its original direction and magnitude slowly while the stator flux is changing rapidly by applying voltage vectors on the stator. From equation 5.3, it is noticed that the electromagnetic torque can be controlled by the angle between the rotor and flux vectors, and the magnitude of stator flux.

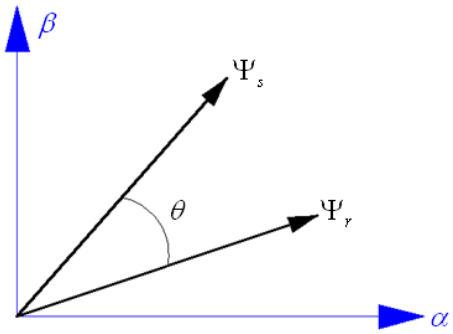

Figure 34: Stator flux and Rotor flux in stationary frame [53]

Because the voltage source inverter consists of six transistors, and eventually it could form 8 switch variables, 6 of them are nonzero vectors and 2 of them are zero vectors. The possible voltage space vectors from the inverter and the corresponding stator flux changes are shown below:

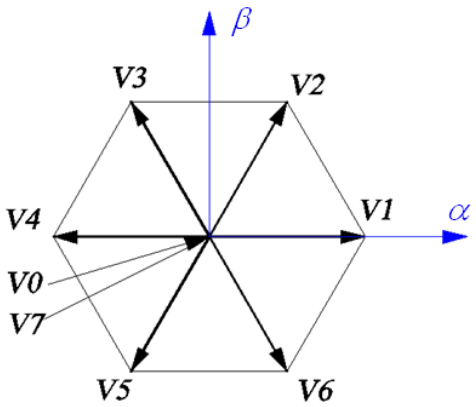

Figure 35: Eight possible voltage vectors formed by a voltage source inverter

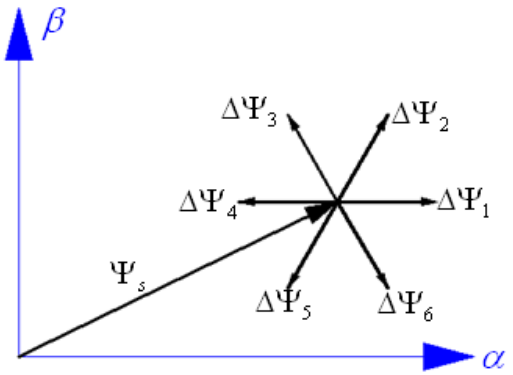

Figure 36: The corresponding stator flux changes

It also can be noticed that if a zero voltage vector is applied on the stator over a given time period, the angle between the rotor and stator flux vectors will decrease. By applying a zero voltage vector, the stator flux vector will stay as it is fixed, but the rotor flux will not be affected, and it keeps rotating as original. This indicates that the torque generated by the induction motor will be decreasing while a zero vector is being applied.

A tangential and a radial incremental variation in the stator flux could be yielded by applying one of the six possible voltage vectors. The tangential variation determines the change of the torque, since the torque of the motor, from equation 5.3, is proportional to the angle between the rotor and stator flux. On the other side, the radial variation of flux determines the change of the stator flux magnitude. Thus both torque and flux control will be achieved, by manipulating the stator flux vector in one of the six possible directions [54].

5.2 Flux Control and Torque Control

Direct torque control system includes two parts: flux direct control, and torque direct control.

5.2.1 Stator Flux Control

Using the voltage model flux observer, the stator flux can be estimated as:

$$\Psi_s(t) = \int_0^t (u_s - R_s i_s)dt \tag{5.4}$$

It can be seen that the flux and torque are calculated from the motor terminal voltages and currents.

The flux hysteresis-controller

Regulate the flux by using a two-level digital output hysteresis-controller and the relations are given below:

$$S_\Psi = 1 \qquad \text{for} \qquad \Delta E_\Psi \geq +\Psi_g \tag{5.5}$$

$$S_\Psi = -1 \qquad \text{for} \qquad \Delta E_\Psi \leq -\Psi_g \tag{5.6}$$

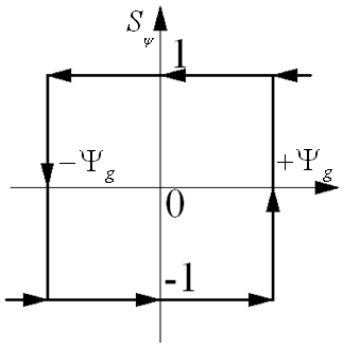

Figure 37: The two-level hysteresis controller for stator flux

where $2\Psi_g$ is the band width of the flux hysteresis-controller. The actual stator flux Ψ_s is constrained within the hysteresis band and it rotates in an anti-clockwise direction while following the command flux in a Z-shaped path [55].

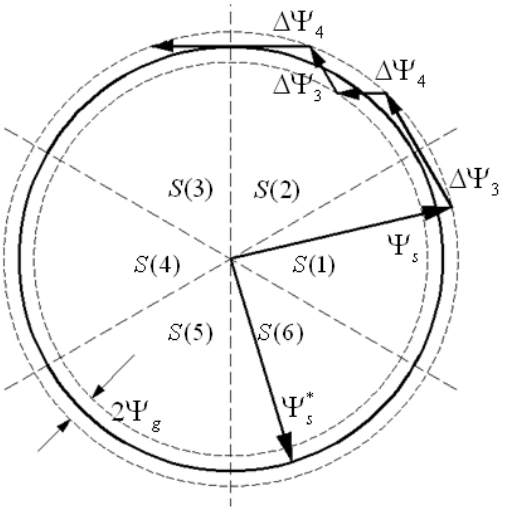

Figure 38: Stator flux trajectory

5.2.2 Electromagnetic Torque Control

The electromagnetic torque can be obtained by following equations:

$$T_e = K_6 \Psi_r \times I_s \tag{5.7}$$

$$T_e = K_6 (\psi_{\alpha s} i_{\beta s} - \psi_{\beta s} i_{\alpha s}) \tag{5.8}$$

The torque hysteresis-controller

The torque is also regulated by a hysteresis-controller. The difference is that it has three levels of digital outputs as follows:

$$S_{Te} = 1 \qquad \text{for} \qquad \Delta E_T \geq +T_g \tag{5.9}$$

$$S_{Te} = -1 \qquad \text{for} \qquad \Delta E_T \leq -T_g \tag{5.10}$$

$$S_{Te} = 0 \qquad \text{for} \qquad \Delta E_T = 0 \tag{5.11}$$

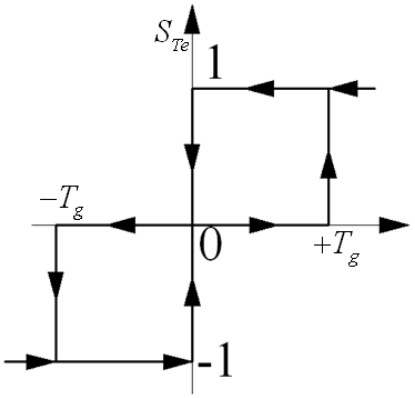

Figure 39: The three-level hysteresis-controller for electromagnetic torque

5.3 Voltage Vector Lookup Table

The voltage vector table receives three input signals, they are: S_Ψ, S_T and S(K). S_Ψ and S_T are digital outputs from the flux hysteresis-controller and torque hysteresis-controller. S(K) is sector number in which the flux vector Ψ_s lies. There are six sectors (each has a $\pi/3$ angle width), as shown in Figure 38. From the lookup table, the appropriate voltage vector for the inverter is then selected based on whether there needs to increase or decrease the torque and stator flux.

Table 3: Voltage vector lookup table [56]

S_{Psi}	S_{Te}	S(1)	S(2)	S(3)	S(4)	S(5)	S(6)
1	**1**	V2	V3	V4	V5	V6	V1
	0	V0	V7	V0	V7	V0	V7
	-1	V6	V1	V2	V3	V4	V5
-1	**1**	V3	V4	V5	V6	V1	V2
	0	V7	V0	V7	V0	V7	V0
	-1	V5	V6	V1	V2	V3	V4

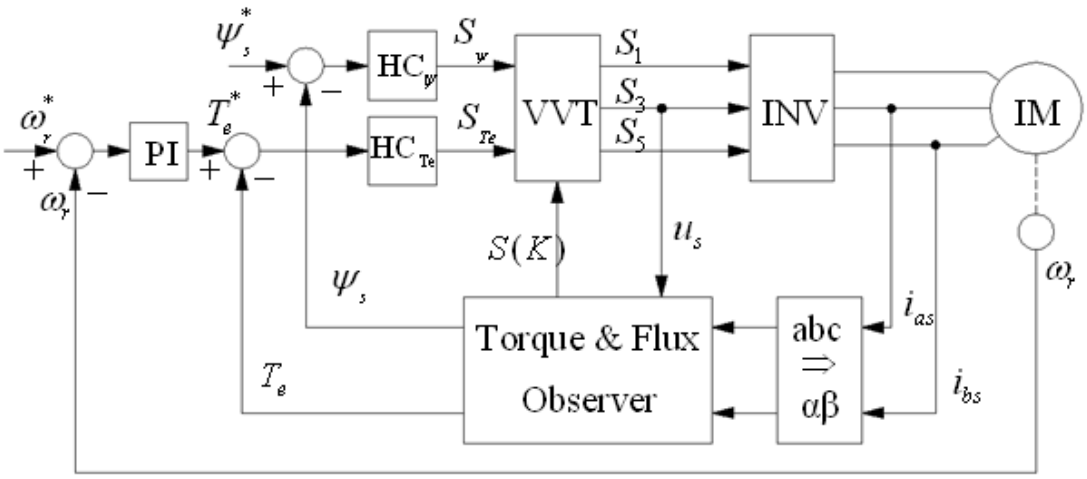

Figure 40: Block diagram of Conventional DTC

5.4 Stator Flux Orientated Sensorless Direct Torque Control

Both FOC and conventional DTC control techniques have been explained in the previous sections, to summarize it, the conventional DTC provides a better dynamic torque response while the FOC provides a better steady state behavior.

But for vehicular applications, both steady state and dynamic performance are important to the system designer. For example, some driving conditions may desire a less strict torque regulation but require a well controlled speed performance. Like cruising mode, it runs for a long period of time at constant speed but requires very little dynamic response. On the contrary, another type of driving condition requires excellent dynamic response, but steady state speed performance could be less important.

The stator flux orientated sensorless DTC is based on conventional direct torque control, so the torque and flux performance can be guaranteed. At the same time the stator flux orientation technique is applied to predict the rotor speed. The flux orientation is a necessary part in FOC and because of this FOC achieves the decoupled currents and shows an excellent speed behavior. Thus, a DTC scheme with the flux orientation technique will provide a well regulated speed performance. At the same time, speed sensor can be eliminated from the system, because the rotor speed can be estimated instead of being measured. The absence of the speed sensor, either optical encoder or hall-effect speed sensor will definitely improve the ruggedness and reduces the cost of the entire system. [57-59]

The relationship between rotor flux and stator flux can be given below, for both d and q components:

$$\psi_{dr} = \frac{L_r}{L_m}\psi_{ds} - \frac{l^2}{L_m} i_{ds} \qquad (5.12)$$

$$\psi_{qr} = \frac{L_r}{L_m}\psi_{qs} - \frac{l^2}{L_m} i_{qs} \tag{5.13}$$

$$l^2 = L_r L_s - L_m^2 \tag{5.14}$$

Next the stator flux is fixed with the synchronous rotating frame, since the d-axis is aligned with the stator flux direction, the flux d and q components can be rewritten as:

$$\psi_{ds} = \psi_s \tag{5.15}$$

$$\psi_{qs} = 0 \tag{5.16}$$

Substitute these into the equation above, we can have:

$$\psi_{dr} = \frac{L_r}{L_m}\psi_s - \frac{l^2}{L_m} i_{ds} \tag{5.17}$$

$$\psi_{qr} = -\frac{l^2}{L_m} i_{qs} \tag{5.18},$$

Then the rotor flux can be calculated out:

$$\psi_r = \sqrt{\psi_{dr}^2 + \psi_{qr}^2} \tag{5.19}$$

$$\theta_{er} = \arctan\frac{\psi_{qr}}{\psi_{dr}} \tag{5.20}$$

And the synchronous can also be calculated out:

$$\omega_e = \frac{d\theta_{er}}{dt} = \frac{d\arctan\dfrac{\psi_{qr}}{\psi_{dr}}}{dt} = \frac{\psi_{dr}\dfrac{d\psi_{qr}}{dt} - \psi_{qr}\dfrac{d\psi_{dr}}{dt}}{\psi_{dr}^2 + \psi_{qr}^2} \tag{5.21}$$

From the conventional DTC theory, the stator flux is given as:

$$\psi_s = \int (u_s - R_s i_s) dt \tag{5.22}$$

From the frequency characteristic, vector Ψ_s is always perpendicular to vector $u_s - R_s i_s$. And since u_s and i_s can be measured from the terminals of induction motor, it is possible to acquire the phase angle of vector $u_s - R_s i_s$, so that the phase angle of Ψ_s can be determined.

If $u_m = u_s - R_s i_s$, the phase angle $\theta_m = \arctan(\frac{u_{\beta s} - R_s i_{\beta s}}{u_{\alpha s} - R_s i_{\alpha s}})$ is shown in the following figure:

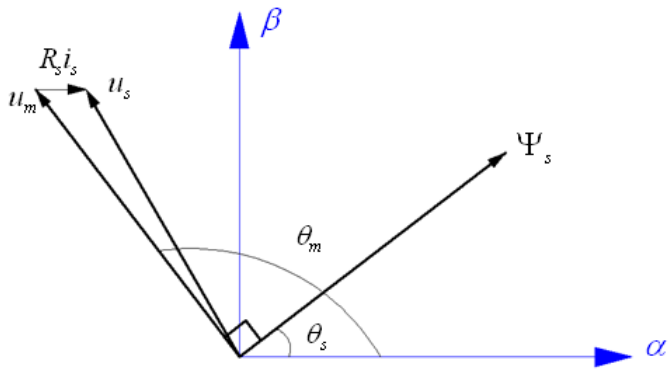

Figure 41: The relationship between stator flux and stator voltage vector

Thus the phase angle of stator flux Ψ_s can be given as:

$$\theta_s = \theta_m - \frac{\pi}{2} \tag{5.23}$$

And then use this angle θ_s in the park transformation. On the other hand, from the theory of FOC, the slip speed is given as:

$$\omega_{sl} = \frac{(1 + T_r p)}{T_r} \frac{i_{qs}}{i_{ds}} \tag{5.24}$$

Thus, using the speed relationship which has been defined in the induction motor modeling section, the rotor speed is give:

$$\omega_r = \omega_e - \omega_{sl} \tag{5.25}$$

Substitute the slip speed ω_{sl} and synchronous speed ω_e :

$$\omega_r = \frac{\psi_{dr} \frac{d\psi_{qr}}{dt} - \psi_{qr} \frac{d\psi_{dr}}{dt}}{\psi_{dr}^2 + \psi_{qr}^2} - \frac{(1 + T_r p)}{T_r} \frac{i_{qs}}{i_{ds}} \tag{5.26}$$

This equation gives the method of estimating rotor speed, after this, the estimated rotor speed will be compared with the reference value and then fed into a PI controller.

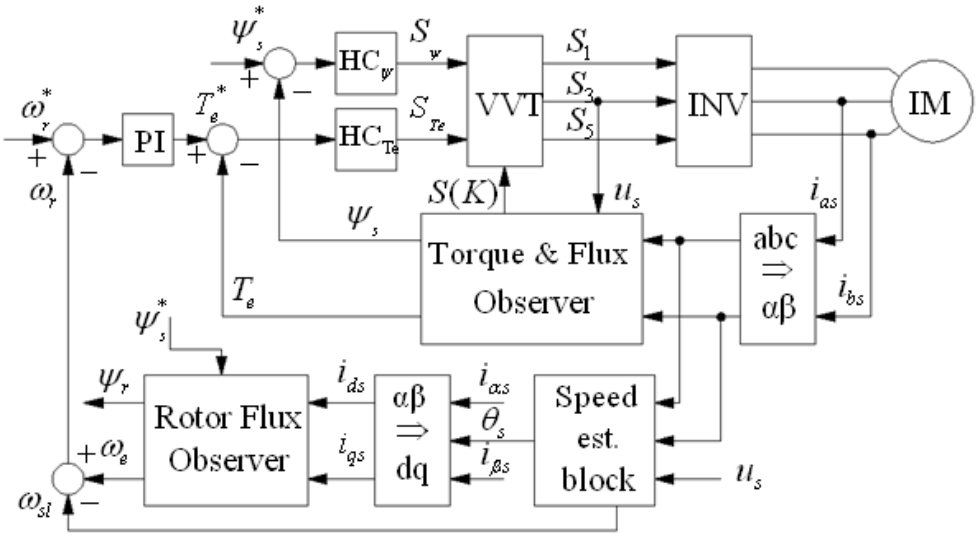

Figure 42: Block diagram of SFO-Sensorless DTC

By using this Stator flux orientated sensorless direct torque control method, the rotor speed, torque and stator flux will be regulated in an entire control system.

5.5 Implement of DTC

For DTC we also need to do the Clarke transformation first. So the figures below show the three phase currents are being transformed into two phase currents.

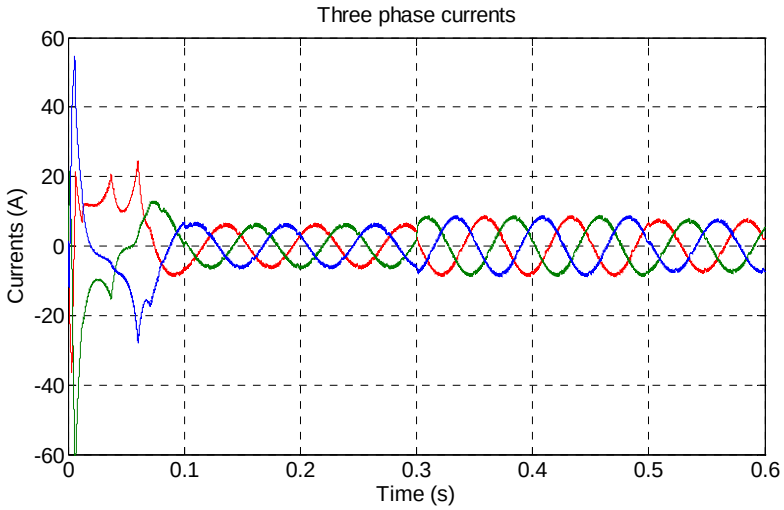

Figure 43: Three phase stator currents in conventional DTC

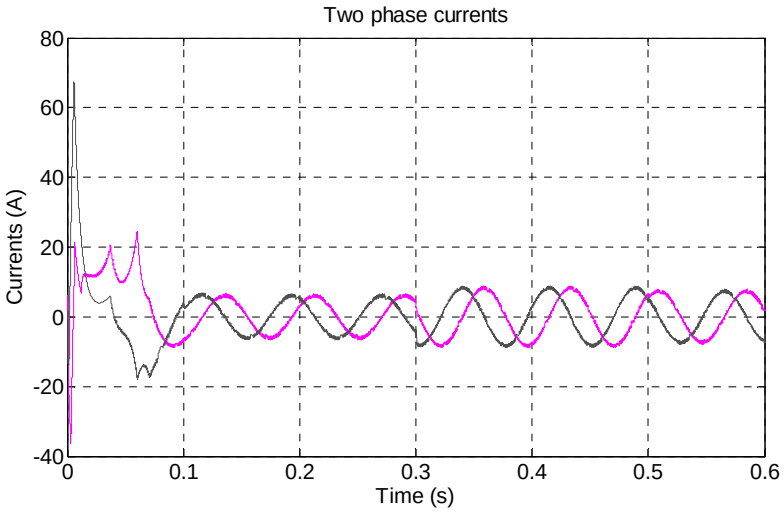

Figure 44: Two phase currents after Clarke transformation in conventional DTC

The most significant characteristic of DTC is that hysteresis torque regulator and hysteresis flux regulator are being applied in the system to control torque and flux directly. So generally speaking, if the regulators are well tuned, the torque response and flux response should be restricted in their boundaries respectively.

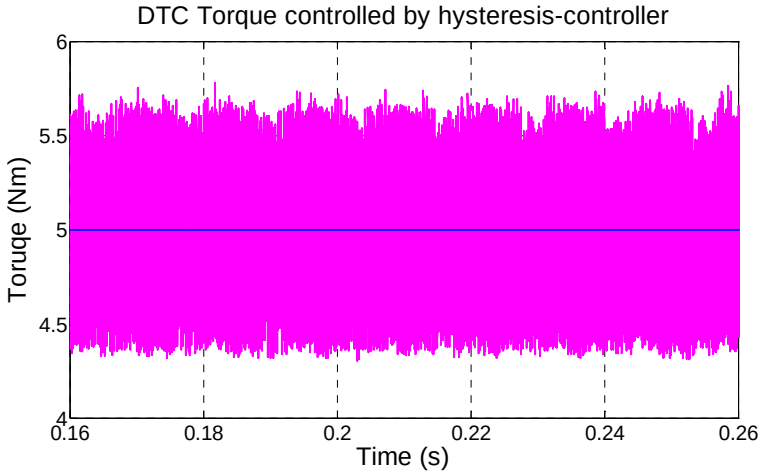

Figure 45: Torque response with command in conventional DTC

The boundary of torque hysteresis controller is set from -0.5 Nm to 0.5 Nm, so from the figure above, we can see that the torque response is well regulated.

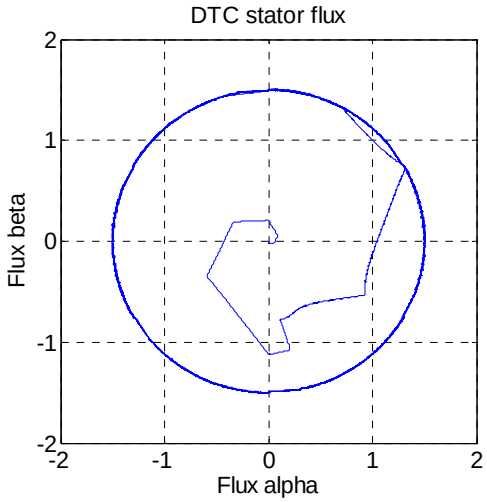

Figure 46: Circular stator flux trajectory in conventional DTC

At the same time, the boundary of flux hysteresis controller is set from -0.005 Wb to 0.005 Wb. At the starting stage, the flux takes a few steps to reach the rated value, and then, it is clear to see that the flux response is well restricted in its boundary. This is the most significant difference between FOC and DTC.

5.6 DTC Summary

Conventional DTC attracts many researchers because of its fast torque response and simple control method [19, 20]. The main features of conventional DTC are summarized as follows [60]:

- There is direct feedback control of torque and stator flux magnitude;
- No feed back current control;
- Flux observer only uses one motor parameter (Rs);
- No vector rotating transformation (Park Transformation);
- There are ripples in flux and torque because of the hysteresis band control.

CHAPTER VI. SIMULATION RESULTS

6.1 Overview

Simulations for both steady state and dynamic condition were carried out to validate the theories in the previous chapters. It is very necessary to test the feasibility of control strategies using simulation before practicing them in hardware. Thus, simulation models of FOC, conventional DTC and Sensorless DTC were built respectively. A 5-hp induction motor is used, and the parameters of this motor are given in the table below. Simulations scripts were written using MATLAB M-script, and simulation models were built using Simulink toolboxes and blocks.

Table 4: Induction motor parameters for simulation

Nominal power (W)	14920	Rotor resistance (ohm)	0.1645
Voltage (line-line) (V)	460	Rotor inductance (H)	0.002891
Frequency (Hz)	60	Mutual inductance (H)	0.1062
Stator resistance (ohm)	0.2761	Inertia (J(kg*m^2))	0.1
Stator inductance (H)	0.002891	Polar number	2

6.2 Simulation Results

Both steady state and dynamic performance are important to the system design engineers no matter what controller is being used. So for any given application, evaluation of the system performance should be considered in both aspects.

6.2.1 Scenario 1: Cruise Mode (Torque verses constant speed)

First of all, it is important to analyze the starting performance. During this starting period, the electric motor needs to produce a relatively high torque in a very short time to accelerate itself. The investigation here is focused on speed response time, fluctuations as well as three phase currents of induction motor.

Then, when the vehicle is running at a constant speed for example in cruise mode, the load on the motor can vary abruptly because of the change of the road conditions. At this kind of state, the vehicle also needs a precise average torque and stable response from the electric motor. Therefore, the investigation is focused on torque fluctuations and current ripples.

In the scenario 1, the speed command and torque command are given below:

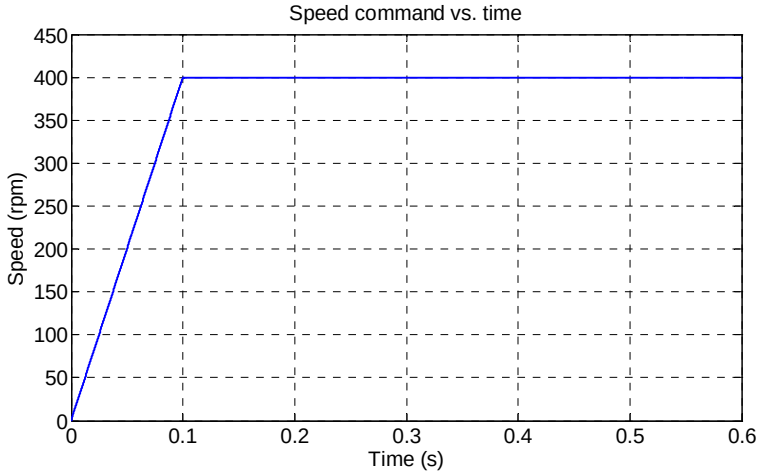

Figure 47: Speed command vs. time in Scenario 1

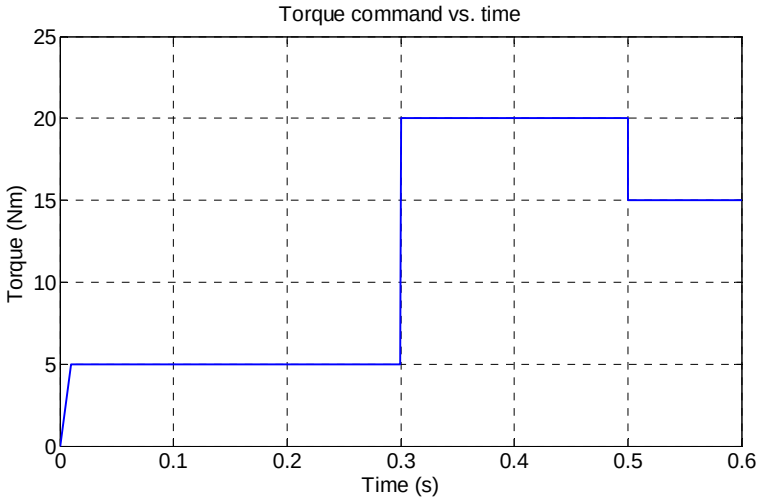

Figure 48: Torque command vs. time in Scenario 1

A ramp signal is used to simulate the vehicle starting behavior, after the motor rotor speed reaches the target value of 400 rpm, it was kept as a constant. At the same time, when the motor was started from standstill with a ramp load torque from 0 to 5 Nm to the steady state speed of 400 rpm. And then, during the constant speed period, the

load was changed to 20 Nm at the time t = 0.3s, and changed again to 15 Nm at t = 0.5s.

The speed response of FOC, conventional DTC and Sensorless DTC:

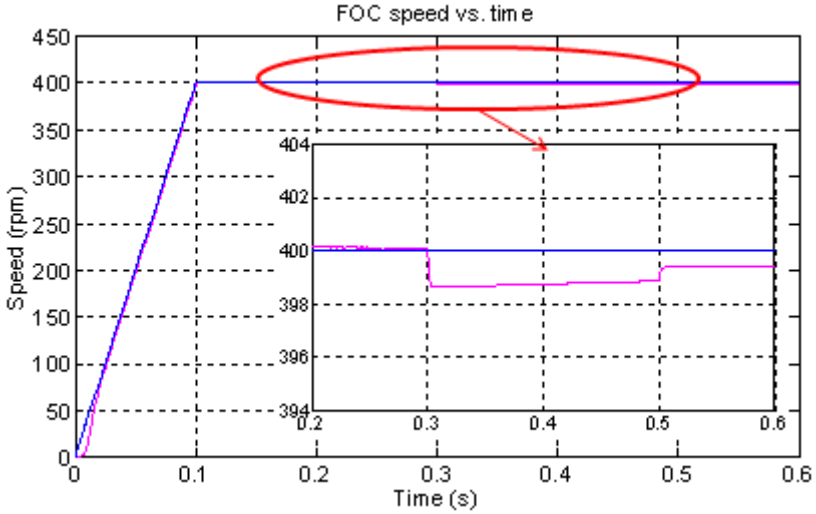

Figure 49: Speed response of FOC in Scenario 1

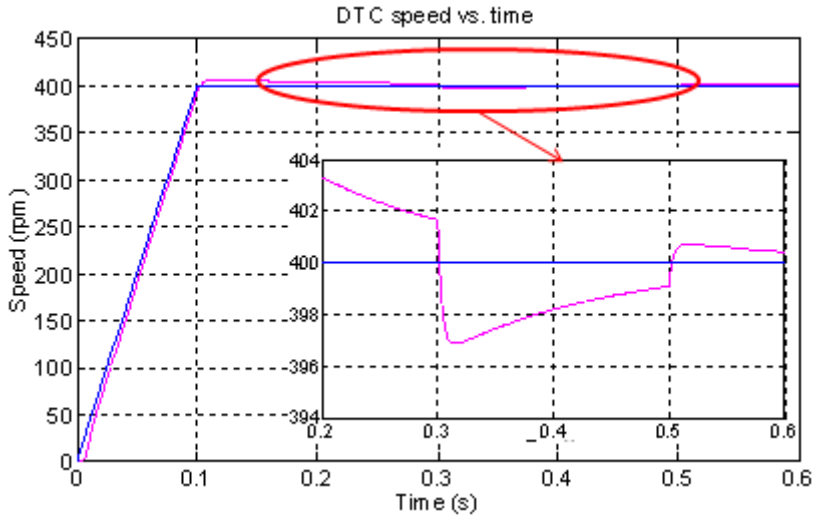

Figure 50: Speed response of conventional DTC in Scenario 1

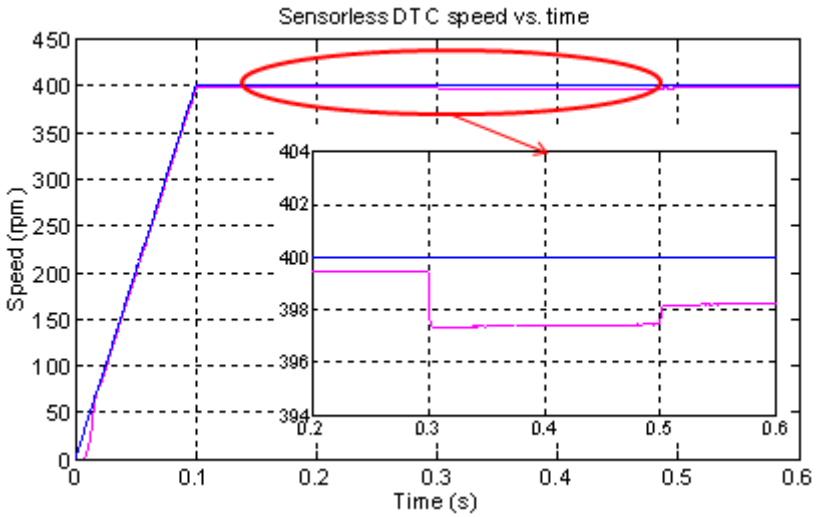

Figure 51: Speed response of SFO-Sensorless DTC in Scenario 1

Generally speaking, for FOC, conventional DTC and sensorless DTC, the speed of any of them is well regulated; there is no spike in speed response curves. It can be seen that as the load torque is suddenly changed, there is a small speed dip, but then it is restored quickly.

From the zoomed in pictures of speed response, we can see that at the time t = 0.1s, the speed response of FOC follows the command very closely, the overshoot is almost 0, for DTC, the overshoot at t = 0.1s is about 5 rpm, and for sensorlees DTC, the error is less than 1 rpm. At the time t = 0.3s when the torque changes, the change of FOC speed response is about 2 rpm while the DTC's is around 6 rpm and sensorless DTC's is around 3 rpm. From this analysis we can summarize up that FOC has the best speed following characteristic among three of them, and sensorless DTC has a better one than the conventional DTC.

The torque response of FOC, conventional DTC and Sensorless DTC:

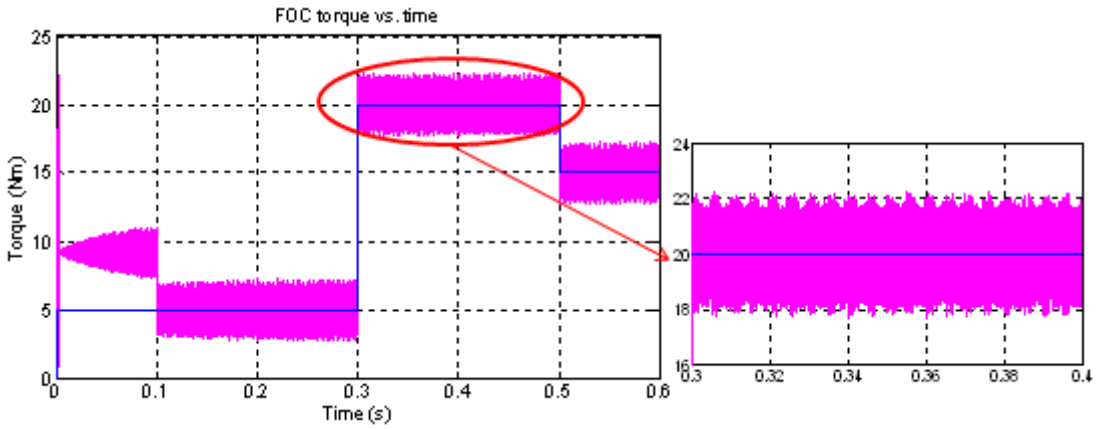

Figure 52: Torque response of FOC in Scenario 1

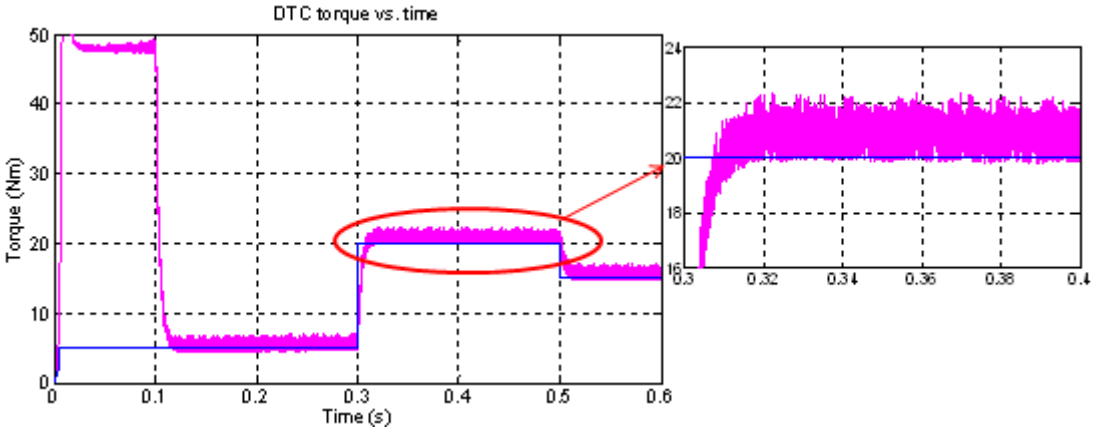

Figure 53: Torque response of conventional DTC in Scenario 1

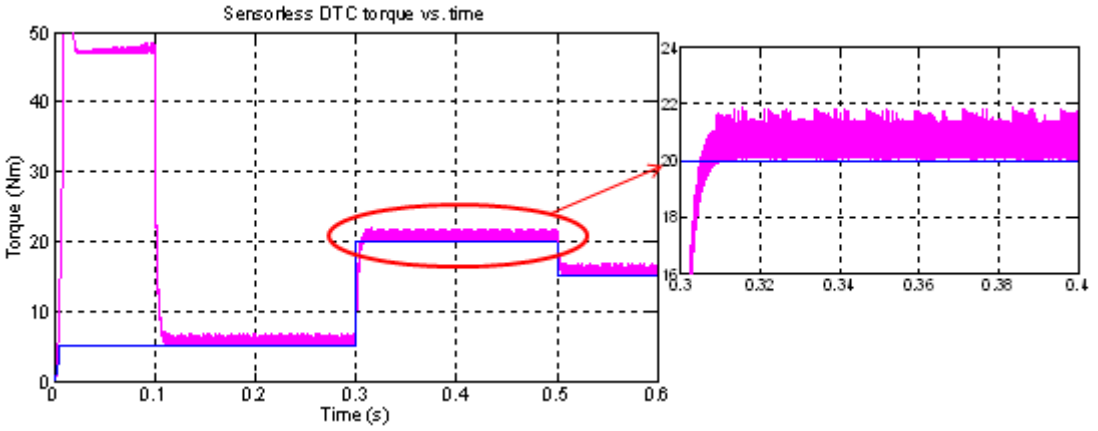

Figure 54: Torque response of SFO-Sensorless DTC in Scenario 1

For the torque responses, at the first stage, a large torque is generated to accelerate the motor. After reaching the target speed, the torque output follows the command closely. In DTC family, either conventional DTC or sensorless DTC, the torque is controlled by a hysteresis controller. By properly adjusting the positive band and negative band of this hysteresis controller, a satisfied torque response will be achieved. From the

simulation result shown above, it is clear to see that the torque response is decent and fast.

From the zoomed picture of torque response, it is clear to see that the torque fluctuations of FOC are restrained within +2 and -2 (Nm) with respect to the torque command. On the other hand, it is noticed that the torque ripples of conventional DTC are restrained in -1 and +1 (Nm) with respect of the command value.

Three phase currents response of FOC, conventional DTC and SFO-Sensorless DTC:

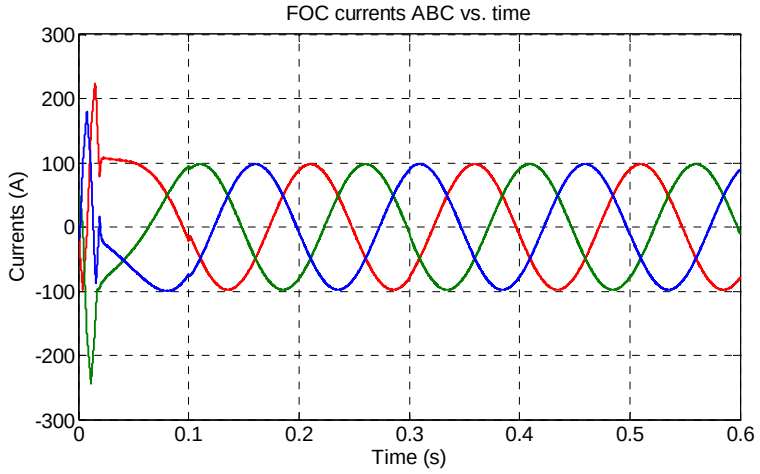

Figure 55: Currents response of FOC in Scenario 1

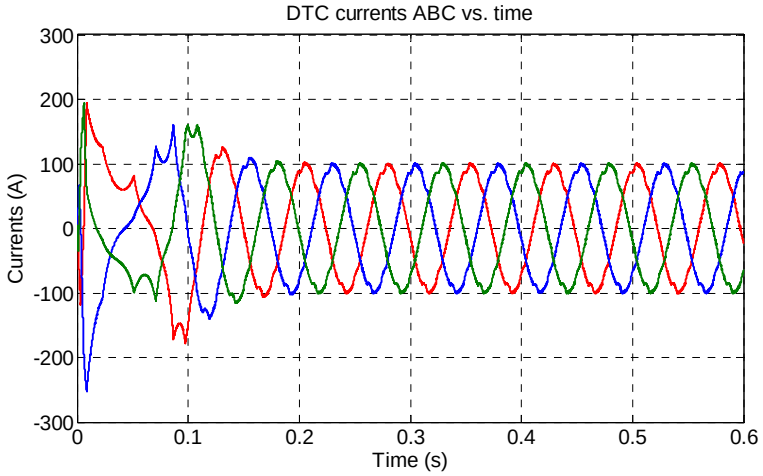

Figure 56: Currents response of conventional DTC in Scenario 1

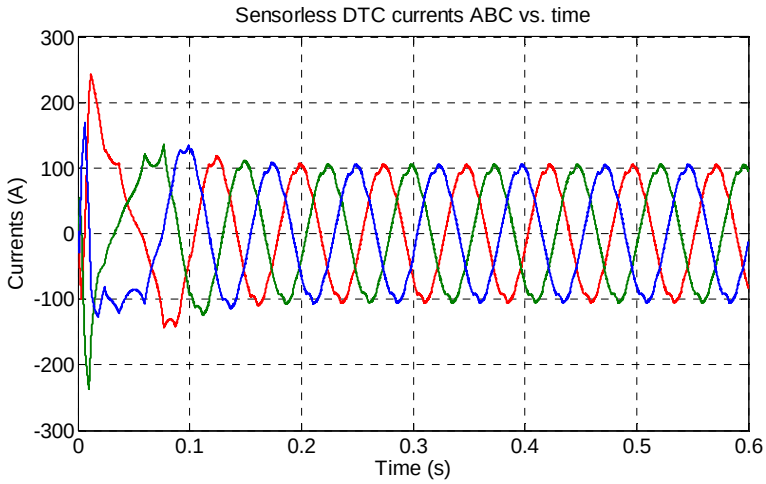

Figure 57: Currents response of SFO-Sensorless DTC in Scenario 1

Figure 55 shows the three phase currents of induction motor using the FOC. Since the FOC is aim at controlling decoupled currents I_{qs} and I_{ds} of the system, so generally speaking, the currents are well regulated. It can be seen that, at the starting stage, three phase currents are constrained within -200 to +200 Amps. After that, the magnitude of the current is kept around 100 Amps.

Figure 56 shows the three phase currents of the induction motor by using conventional DTC, because in this control method, there is no current regulator, so the performance of current at the starting stage is not as good as that in FOC. Obviously to see, the current shape at the starting stage is not well controlled, after about 0.1 second later the currents come back to normal as soon as the motor reaches the steady state. Same phenomena are seen in Figure 57 for sensorless DTC.

6.2.2 Scenario 2: City Driving Mode (Torque verses varying speed)

Unlike the cruise mode, in this scenario, instead of keeping the speed as a constant all the time, it is more realistic to use different demands for the city driving mode; the speed of the motor is changing with time.

In this scenario, the speed command and torque command are given below:

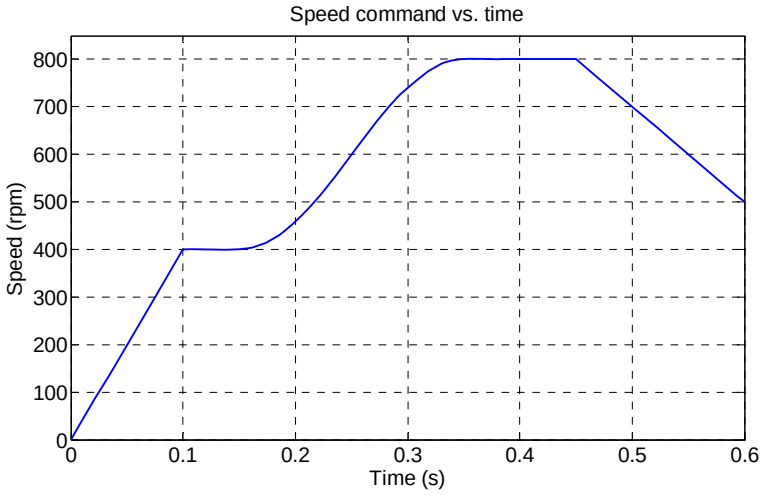

Figure 58: Speed command vs. time in Scenario 2

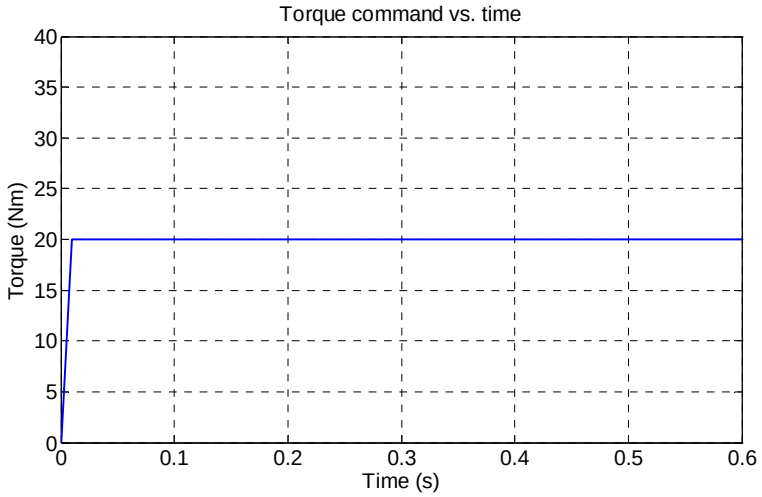

Figure 59: Torque command vs. time in Scenario 2

A ramp signal is also used here to simulate the vehicle starting behavior, after the motor rotor speed reaches the target value of 400 rpm, a sinusoidal speed command is applied, the speed is increased from 400 to 800 rpm, and then, a negative ramp is applied to reduce the speed from 800 to 500 rpm. A torque ramp is used at the beginning for a very short time, after that it was kept as a constant value at 20 Nm.

The speed response of FOC, conventional DTC and SFO-Sensorless DTC:

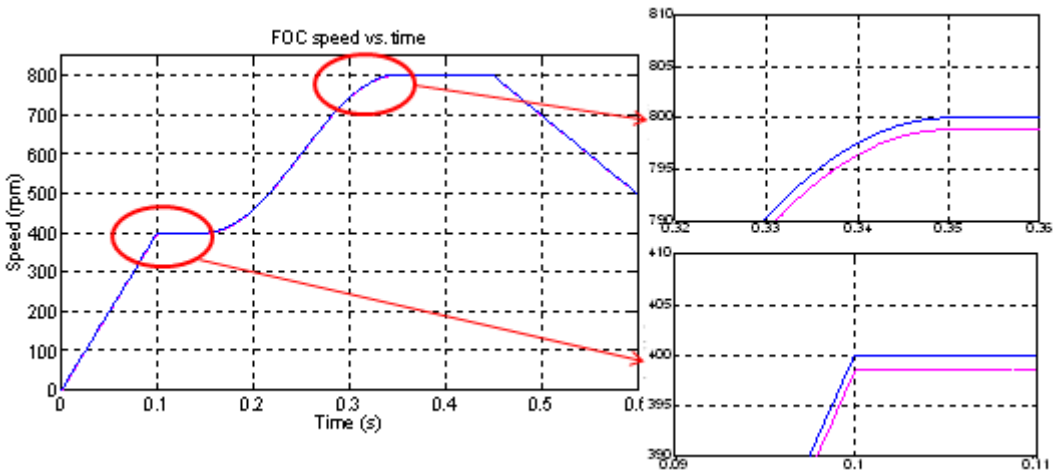

Figure 60: Speed response of FOC in Scenario 2

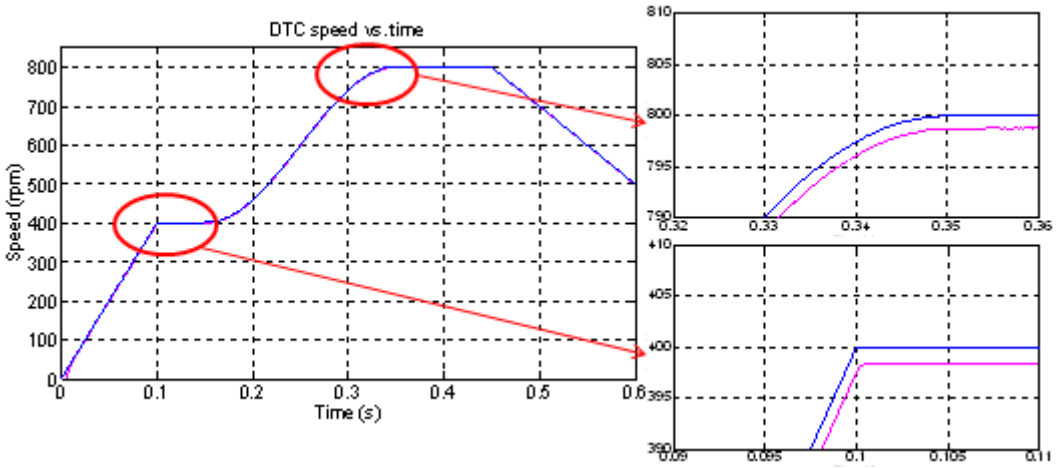

Figure 61: Speed response of conventional DTC in Scenario 2

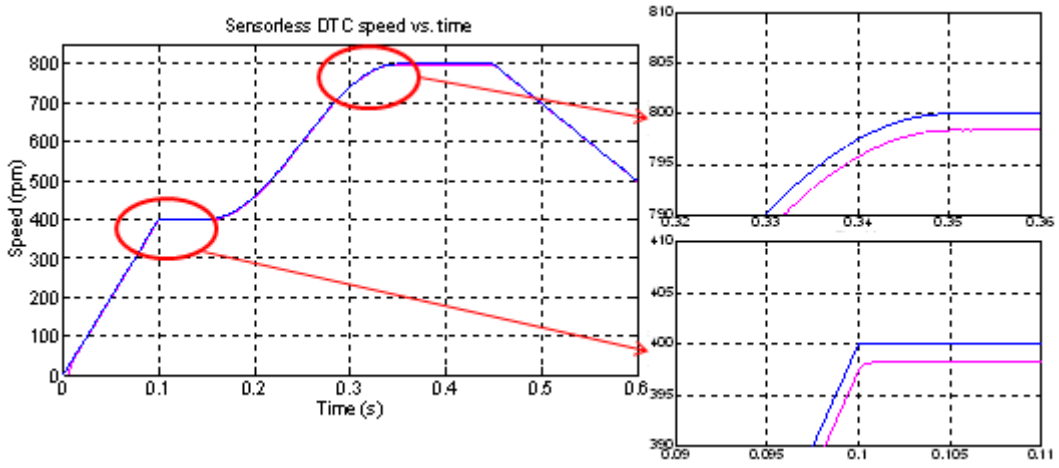

Figure 62: Speed response of SFO-Sensorless DTC in Scenario 2

Figure 60-62 show the speed simulation result for FOC, conventional DTC and sensorless DTC, generally speaking, the speed is well controlled, there is no spike in the entire curve, and from the zoomed in pictures, we can see that both the overshoot

and the steady error in each control algorithm are small enough. So in scenario 2, all the control methods have really good speed response.

The torque response of FOC, conventional DTC and Sensorless DTC:

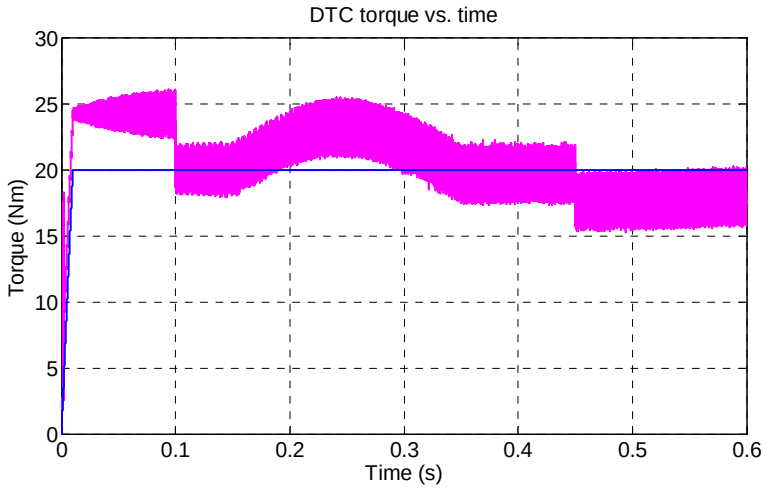

Figure 63: Torque response of FOC in Scenario 2

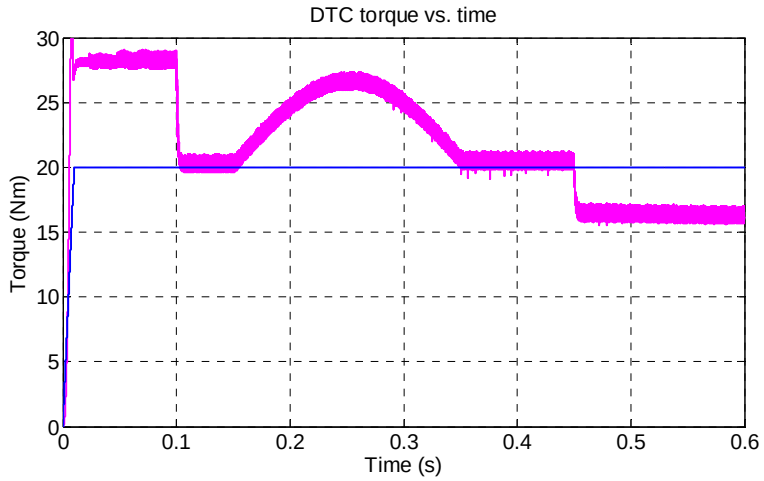

Figure 64: Torque response of conventional DTC in Scenario 2

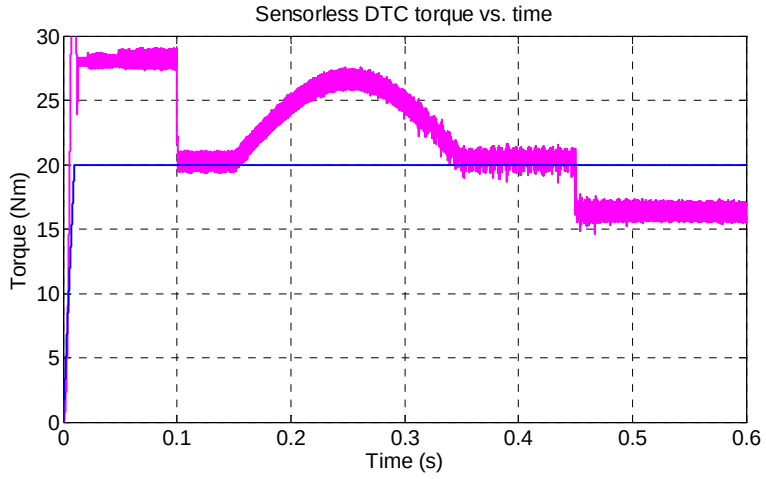

Figure 65: Torque response of SFO-Sensorless DTC in Scenario 2

The corresponding torque response is shown above, from t = 0s to t = 0.1s, this is the starting stage, a large constant torque is required, from t = 0.15s to t = 0.35, the motor speed is increasing sinusoidally, a torque larger than the command is needed to accelerate the motor, from t = 0.45 to t = 0.6, a torque smaller than the command is generated, since the motor needs to decrease the speed. The same conclusion as the previous will be obtained that conventional DTC and sensorless DTC have a better torque performance and less fluctuation than that of FOC.

Three phase currents response of FOC, conventional DTC and Sensorless DTC:

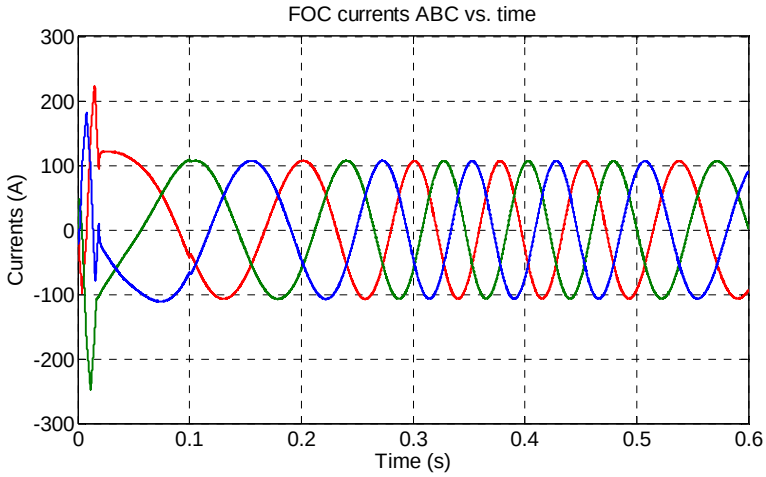

Figure 66: Currents response of FOC in Scenario 2

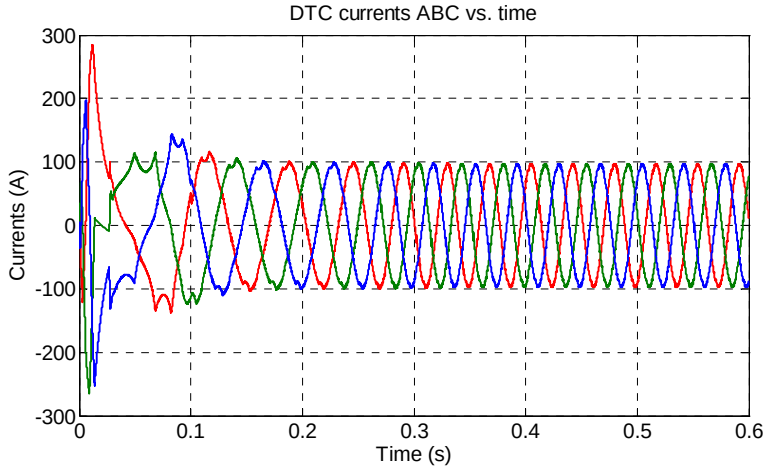

Figure 67: Currents response of conventional DTC in Scenario 2

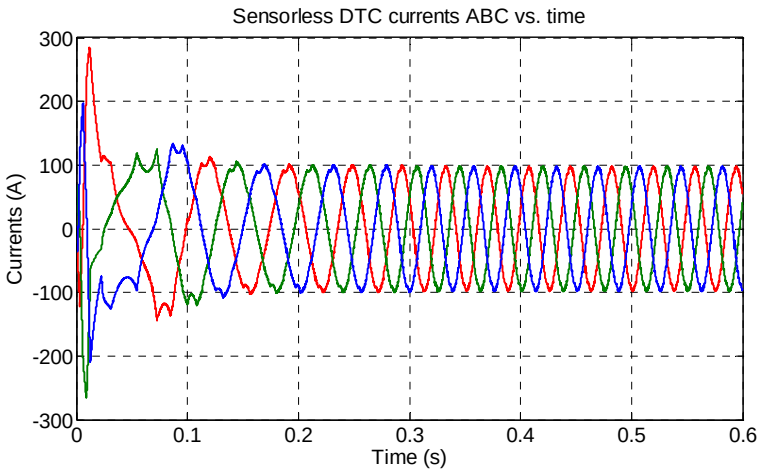

Figure 68: Currents response of SFO-Sensorless DTC in Scenario 2

For the current responses, the same conclusions can be achieved that FOC provides the best current performance.

CHAPTER VII. EXPERIMENTAL

7.1 Overview

Experiments are significant step in engineering study. It has been proved from the simulation results that induction motors operated with FOC will have good steady state and operated with conventional DTC will have good dynamic performance if properly tuned. To further prove feasibility and verify the theoretical analysis, experiments were carried out under different conditions to test the control strategies. In this chapter, a detailed experimental setup procedure will be introduced. Steady state performance data and dynamic experiments results will be analyzed and presented.

7.2 Experiment Setup and Hardware Components

This experiment requires high quality complex equipments. Besides integrating the electrical motor with flywheel, inverter, digital signal processor, measurement instruments and peripheral circuits need to be carefully tuned. The test bench implemented in this research is explained by the schematic in Figure 69.

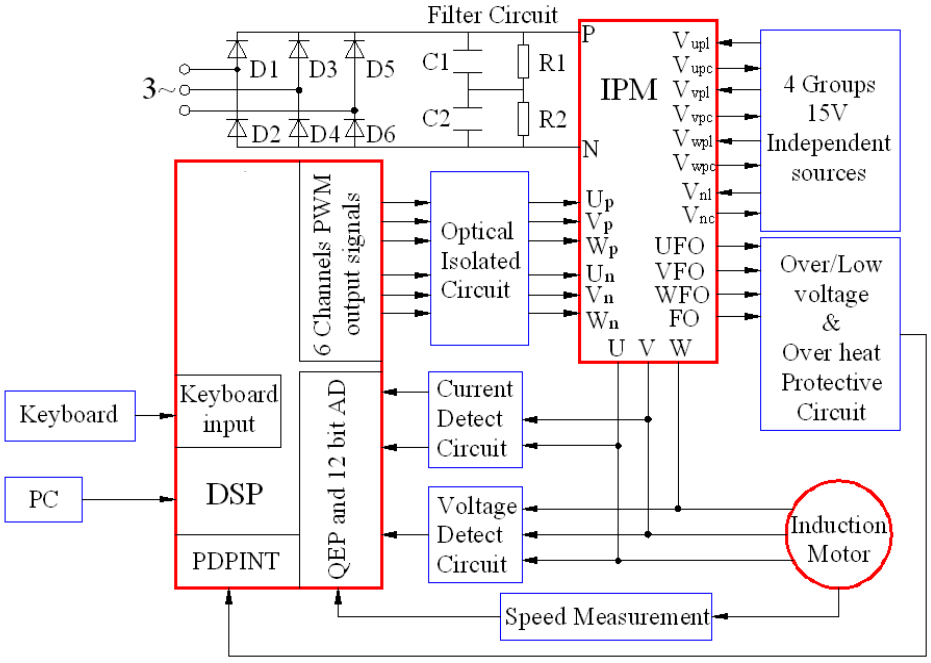

Figure 69: Hardware schematic diagram of induction motor control system

7.2.1 AC Induction Motor and Flywheel

A 15-hp induction motor is used for experimental verification. The nominal DC main bus voltage is 60V and the nominal current is 100 Amps at the maximum speed of 6000 rpm. A flywheel is connected to the motor in the test bench as an inertia dynamometer due to its simplicity and ease of implementation. By knowing the geometry and mass of this flywheel, it is possible to calculate the torque required to accelerate the flywheel. Thus, this flywheel could be used as a load and to simulate the dynamic torque for the system.

7.2.2 Intelligent Power Module (IPM)

To actuate the induction motor, a standardized, research grade inverter and some necessary peripherals were used in the system to test the control algorithms. The inverter is an IGBT-based design (rated at 600V and 150A per phase), with current and voltage sensing. It has a 7-pack Powerex IGBT and is called intelligent Power Module (IPM). The IPM module contains circuitry for shutting down the switching signals in the event of an over current or over temperature condition. The integration of the electrical bus between switches as well as the internal gate drivers makes the IPM an extremely reliable switching solution.

A peripheral circuit is necessary for driving the IPM. Switching signals fed to IPM require 15V to turn on and 0v to turn off. Fault signals are generated by the IPM at the same voltage levels. An interface board was designed for the IPM to optically isolate the switching signals for each phase and the output fault signals. At the same time the interface board was designed to connect the DSP developing board with the IPM module.

7.2.3 Digital Signal Processor (DSP)

The control unit in this system was performed by using a commercialized developing

board for which the main processor is a Texas Instruments Digital Signal Processor (DSP). It is designed specifically for multiphase motor applications using PWM/SVPWM techniques. The advantage of this module lies in its programming flexibility and high efficiency.

The computer communicates with the DSP through a USB connection attached to an emulator; and the emulator is connected to the DSP through a JTAG port. The DSP software development platform is provided by Texas Instruments Code Composer Studio integrated development environment, which supports the ANSI-C language code standard.

7.2.4 Current Sensor, Voltage Sensor, and Speed Sensor

Two currents, phase A and B are sampled with the built-in analog to digital converter on the Texas Instruments DSP. A measurement of the DC bus is sampled with a third A/D conversion. A peripheral circuit was constructed for the current samples with two 200 Amps current sensors and four Texas Instruments low noise operational amplifiers. The current signal is offset and scaled for DSP interface. The operational amplifiers were selected based on the requirement of the DSP for a low impedance signal to result in accurate A/D conversions. On the other hand, another peripheral circuit was designed to process the DC bus voltage for measurement using a voltage sensor. This circuit isolates the bus from the DSP and scales the signal to the 0-3V range accepted by the DSP. Finally, a power supply was built for the current sampling board providing 15V, 0V, and -15V.

Speed measurements were obtained from the built in optical encoder. The optical encoder's disc is made of plastic with transparent and opaque areas. A light source and photo detector array reads the optical pattern which result from the disc's position at any one time. Two output signals are generated from the optical encoder and usually two output wave forms are 90 degrees out of phase, which indicates the rotational

direction. The signals can be read by QEP module on DSP, so that the angular speed of the motor shaft can be calculated in software easily.

7.3 Experimental Results

The experiments are focusing on investigating the current response, torque response and flux response in order to validate and evaluate the dynamic performance and steady performance of FOC and DTC.

This figure shows the three phase currents when the induction motor running at a constant speed in a stable condition. It can be seen that the current is well shaped.

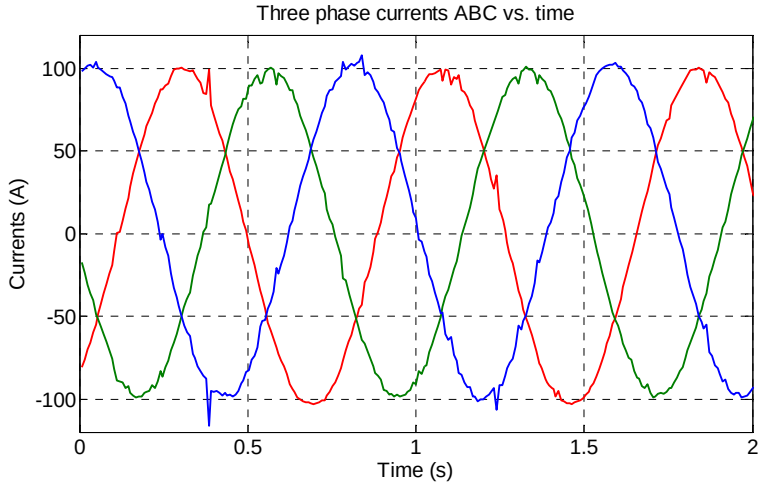

Figure 70: Experimental three phase stator currents in FOC

And next, three phase currents are transferred into two phase using the Clarke transformation.

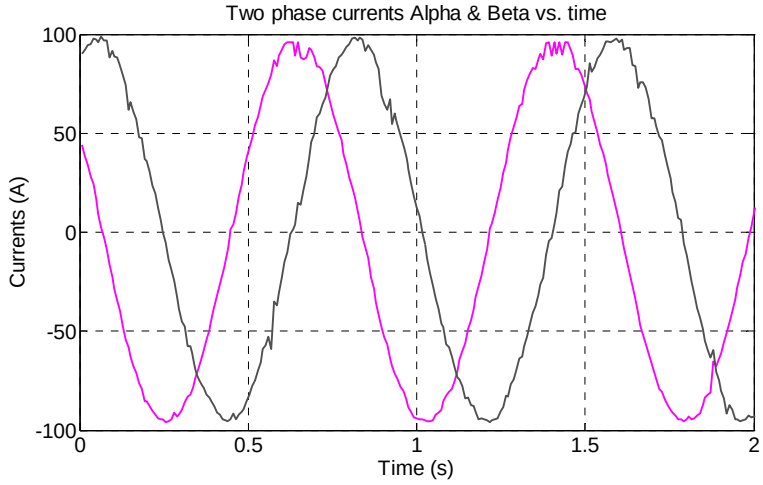

Figure 71: Experimental two phase currents in FOC

To completely decoupled the flux and torque in induction motor, stator currents which have been shown above, still need to be transferred from synchronous rotating frame to flux oriented rotating frame. So the Park transformation is applied here, and decoupled current I_{ds} and I_{qs} are shown below.

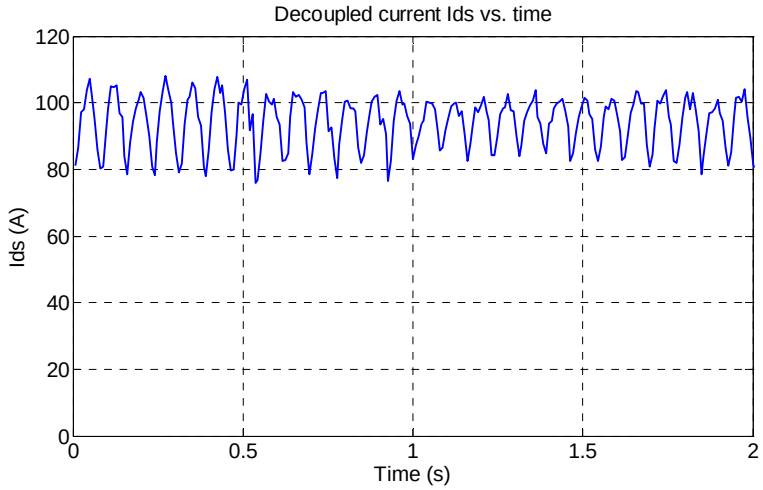

Figure 72: Experimental decoupled current I_{ds} vs. time

From the decoupled current I_{ds}, we can see that it fluctuates from approximately 80A to 110A, which means the rotor flux is fluctuating a little bit when the motor is operating, since the magnitude of original three phase currents is 100A, so the fluctuation of this decoupled current is considered as reasonable.

On the other hand, another decoupled current I_{qs} is shown below:

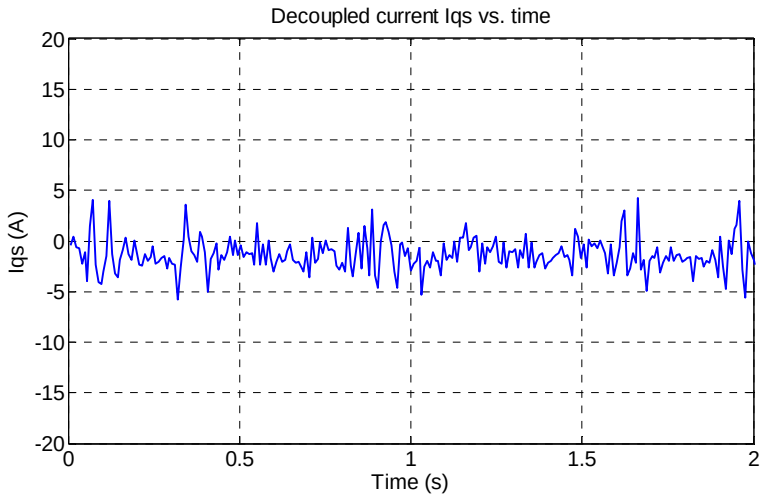

Figure 73: Experimental decoupled current I_{qs} vs. time

These experimental results are acquired under the condition of zero load, so

theoretically the decoupled current I_{qs} should be around zero. From the figure of I_{qs} it is clear to see that the current remains around 0 while the motor is operating.

After decoupling the stator currents into I_{ds} and I_{qs}, two PI controllers are employed to regulate the currents with respect to reference values. The outputs of the current PI controller are then fed into the SVPWM generating module in the program; accordingly, desired PWM voltage signals will be generated. The figure below shows the SVPWM phase voltage output waveform.

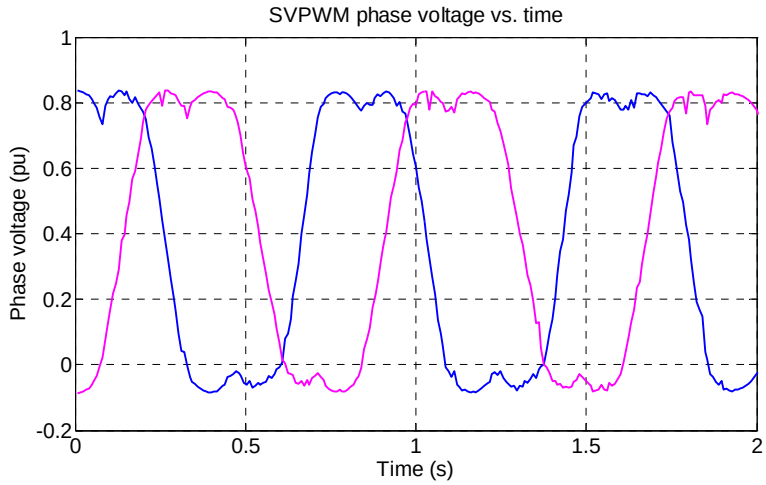

Figure 74: Experimental SVPWM phase voltage waveform

The following figures are the experimental results for DTC. The zero load condition is also tested in the hardware test bench for DTC, so the experimental result for torque response is given below:

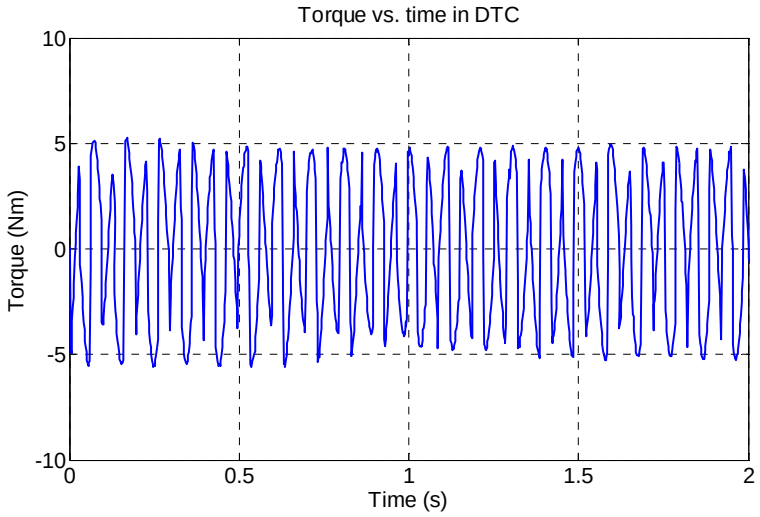

Figure 75: Experimental torque response for DTC

Because hysteresis controller is used in the DTC method for regulating the torque, as the results shown in the figure indicates that the torque fluctuations are restricted in the -5 and -5 Nm boundary.

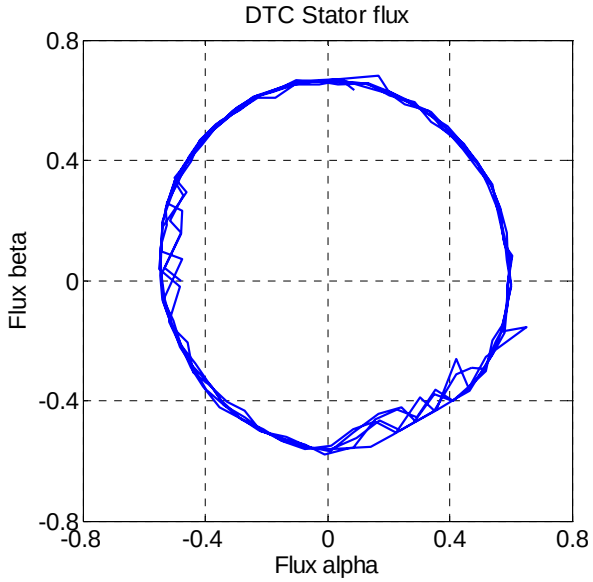

Figure 76: Experimental stator flux trajectory in DTC

In DTC method, the stator flux is also controlled by a hysteresis controller, so that the stator flux will be restrained in the positive and negative boundaries along the reference trajectory.

As Figure 76 indicates, the reference trajectory magnitude is 0.5 wb and the hysteresis

boundaries are -0.01 and 0.01. It is clearly to see that most of time the stator flux is well controlled inside the designed range.

7.4 Comparison Between Simulation Results and Experimental Results

It is very necessary to compare the simulation results with the experimental ones. For one thing we can prove that the experimental process and results are trustable, for another, the simulation modules can be testified as correct.

The decoupled current I_{ds} and I_{qs} in FOC

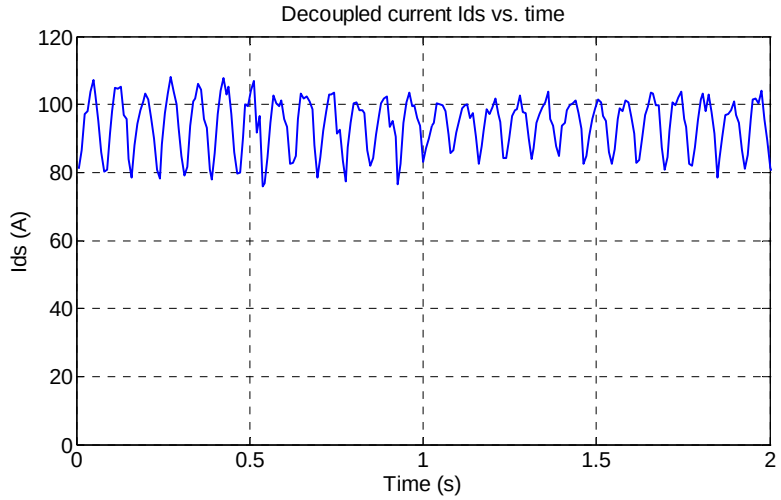

Figure 77: Decoupled current Ids in experiment

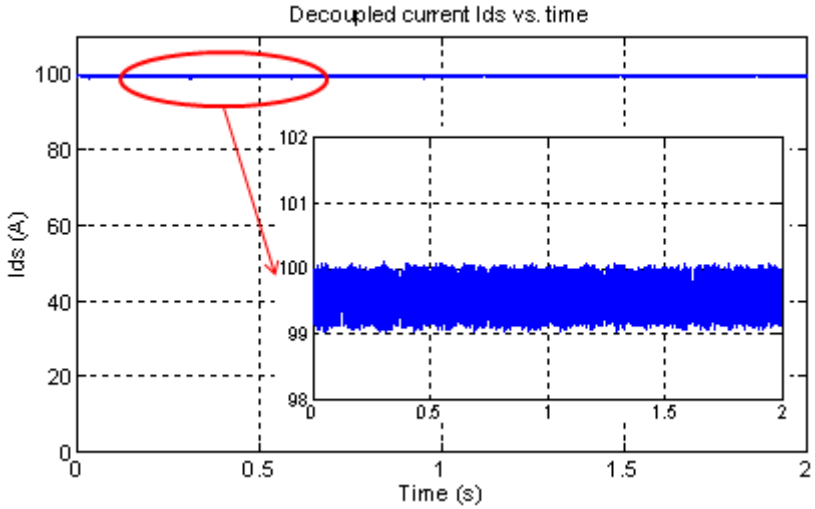

Figure 78: Decoupled current Ids in simulation

As we can see from the above Figure 77 and 78, in the simulation, the decoupled current I_{ds} is kept around 100 A with a fluctuation from 99 to 100 Amps, meanwhile, in the experimental result, the decoupled current I_{ds} is maintained around 100Amps with a fluctuation from 80 to 100 Amps. So generally speaking, the experimental results match the simulation ones.

For another decoupled current I_{qs}, the comparison is shown as follows:

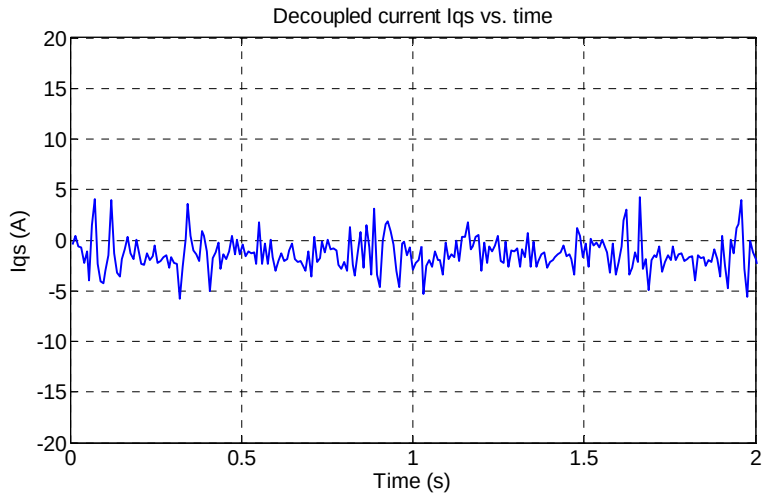

Figure 79: Decoupled current Iqs in experiment

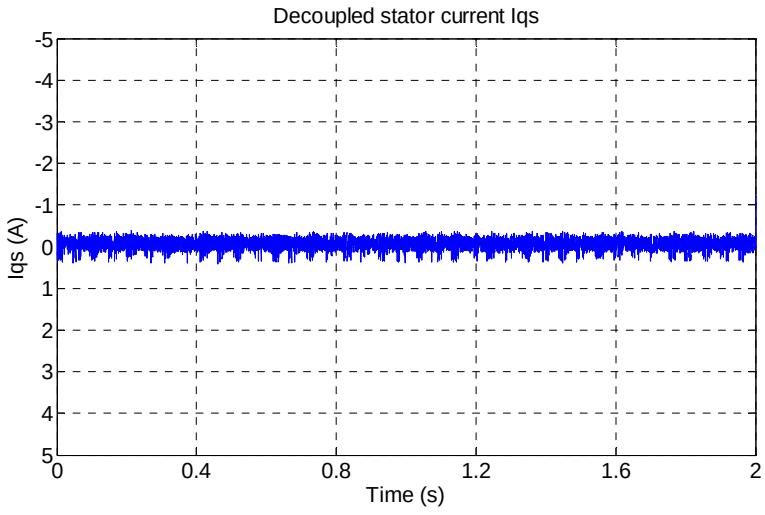

Figure 80: Decoupled current Iqs in simulation

This decoupled current is responsible for generating the torque, since the test condition is zero load, so this current is supposed to maintain around zero. The

experimental results are coinciding with simulation results.

The stator flux comparison in DTC

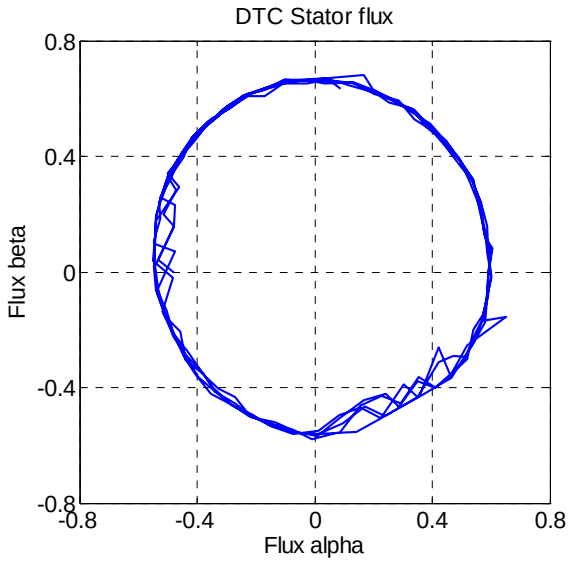

Figure 81: DTC stator flux trajectory in experiment

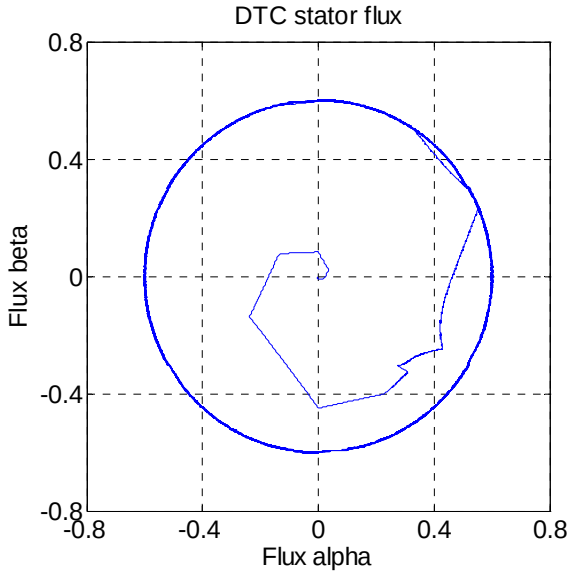

Figure 82: DTC stator flux trajectory in simulation

From these two figures we can see that the hysteresis controller for stator flux in both simulation and experiments is working fine.

The torque comparison in DTC

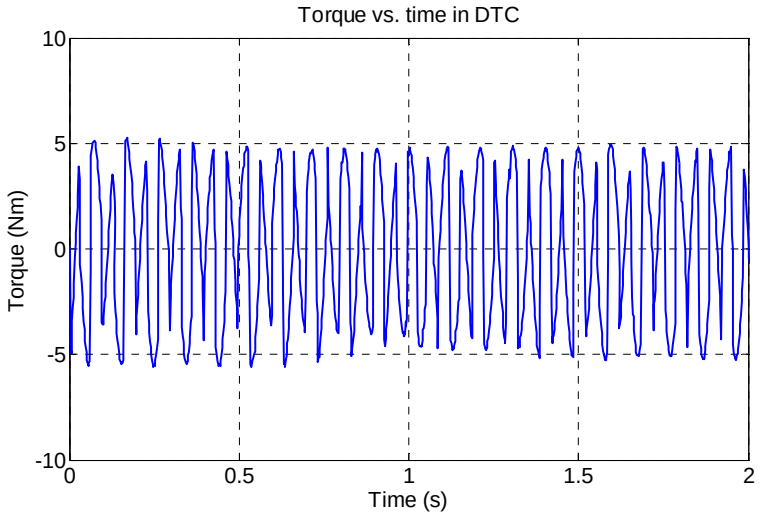

Figure 83: DTC torque response in experiment

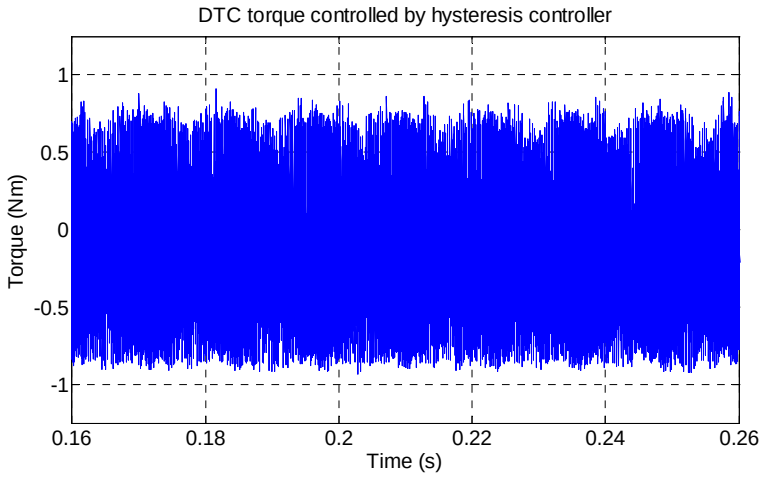

Figure 84: DTC torque response in simulation

Under the zero load condition, the hysteresis controller for torque in both simulation and experiments is also working very well. The same hysteresis boundary was set for both simulation and experiment. But due to the imperfect experimental conditions, the results from the experiment have larger fluctuations than the results in simulations.

CHAPTER VIII. CONCLUSION AND FUTURE WORK

8.1 Conclusion

The results from the simulations have clearly shown that FOC has the best steady performance and best speed following characteristic while conventional DTC and sensorless DTC have a better dynamic performance. At the same time, stator flux oriented sensorless DTC combines the advantages of FOC and conventional DTC, and results in a control method which maintains a good dynamic response as well as a decent steady state performance.

In two simulation scenarios, the induction motor is operated in a cruise mode and a city driving mode, the investigation is focused on the speed response, fluctuations and the stator currents of the induction motor. In addition to that, the load added on the motor is altered twice when the motor is running at the constant speed in cruise mode, so the investigation is also focused on torque response and fluctuations.

Generally speaking, satisfied speed responses are obtained from FOC, conventional DTC and sensorless DTC. The results have clearly shown that as the load torque is suddenly changed, there is a small speed dip, but it is restored quickly. For the torque response, in DTC family, no matter conventional DTC or sensorless DTC, the torque is controlled by a hysteresis controller, so that a better torque performance with less fluctuation is shown in both conventional DTC and sensorless DTC. Because in the conventional DTC and sensorless DTC there is no current regulator, so the performance of stator currents at the starting stage is not as good as that in FOC.

8.2 Recommendation and future work

In this thesis, three control methods of an induction motor: FOC, conventional DTC and stator flux orientated DTC are introduced and compared in simulations, but only FOC and conventional DTC have been validated in the hardware experiments. The

last one stator flux oriented sensorless DTC has not been fulfilled in experiments yet. It is very necessary to test this control method in hardware as well, in order to prove the conclusions obtained from simulations results are consistent with experimental results.On the other hand, due to the limited time, some experiments such as speed following test and load varying driving test are not finished yet. It is also very necessary to complete these experiments to compare three control algorithms in some more realistic hardware conditions.

During both simulation and experiment, it is clearly noticed that the starting behaviors of an induction motor is very important for the entire system. Because of a large torque is needed to accelerate the motor at the very beginning, a relatively large stator current will be generated accordingly. In the hardware experiments this large current is physical provided by the IPM inverter and have to go through the semiconductor circuits inside the IPM. If the current at the starting stage goes too large, the IPM and some other peripheral power devices may have the risk to be damaged. Therefore, how to regulate the currents and together with other variables in the induction motor at the very beginning is a critical issue. More studies need to be done regarding this topic to improve the hardware system reliability and dynamic performance.

The efficiency of three control methods needs to be further investigated. In this thesis, the speed response, torque response and stator currents response are discussed thoroughly, but the efficiency analysis is not included. It is also very necessary to evaluate the efficiency of each control method and present a specific comparison.

At last, some parts of the experimental setup still need to be improved. The parameters of the induction motor used in this test bench still need to be estimated. Some parameters are not precisely known and some parameters may vary with different operating conditions. Compensations regarding the motor parameters need to be further considered in the software program.

REFERENCES

1. J.M. Miller, *Propulsion Systems for Hybrid Vehicles*, London: The Institution of Electrical Engineers, 2004.
2. M. Ehsani, Y. Gao, S. E. Gay, and A. Emadi, *Modern Electric, Hybrid Electric, and Fuel Cell Vehicles: Fundamentals, Theory, and Design*, Boca Raton: CRC Press, 2005.
3. M. Zeraoulia, M. E. H. Benbouzid, and D. Diallo, "Electric motor drive selection issues for HEV propulsion systems: A comparative study," *IEEE Trans. on Vehicular Technology*, vol. 55, pp. 1756-1764, Nov. 2006.
4. Husain, *Electric and Hybrid Vehicles - Design Fundamentals*, Boca Raton: CRC Press, 2003.
5. S. Henneberger, U. Pahner, K. Hameyer, and R. Belmans, "Computation of a highly saturated permanent magnet synchronous motor for a hybrid electric vehicle," *IEEE Trans. on Magnetics*, vol. 33, part 2, pp. 4086-4088, Sept. 1997.
6. B. Stumberger, A. Hamler, M. Trlep, and M. Jesenik, "Analysis of interior permanent magnet synchronous motor designed for flux weakening operation," *IEEE Trans. on Magnetics*, vol. 37, part 1, pp. 3644-3647, Sept. 2001.
7. Online source, available at http://en.wikipedia.org/wiki/Electric_motor.
8. M. Krishnamurthy, C. S. Edrington, A. Emadi, P. Asadi, M. Ehsani, and B. Fahimi, "Making the case for applications of switched reluctance motor technology in automotive products," *IEEE Trans. on Power Electronics*, vol. 21, pp. 659-675, May 2006.
9. C. S. Edrington, M. Krishnamurthy, and B. Fahimi, "Bipolar switched reluctance machines: A novel solution for automotive applications," *IEEE Trans. on Vehicular Technology*, vol. 54, pp. 795-808, May 2005.
10. S. Wang, Q. Zhan, Z. Ma, and L. Zhou, "Implementation of a 50-kW four-phase switched reluctance motor drive system for hybrid electric vehicle," *IEEE Trans. on Magnetics*, vol. 41, part 2, pp. 501-504, Jan. 2005.

11. K. M. Rahman, B. Fahimi, et al., “Advantages of switched reluctance motor applications to EV and HEV: Design and control issues,” *IEEE Trans. on Industry Applications*, vol. 36, pp. 111-121, Jan. -Feb. 2000.
12. Online source, available at http://en.wikipedia.org/wiki/Reluctance_motor.
13. Andrzej M. Trzynadlowski, *Control of Induction Motors*, Academic Press, A Harcourt Science and Technology Company, USA, 2001.
14. Online source, available at http://en.wikipedia.org/wiki/Induction_motor.
15. D. H. Lee, Z. G. Lee, J. Liang, and J. W. Ahn, “Single-phase SRM drive with torque ripple reduction and power factor correction,” *IEEE Trans. on Industry Applications*, vol. 43, pp. 1578-1587, Nov. -Dec. 2007.
16. F. Blaschke, “The principle of field orientation as applied to the new Transvector closed loop control system for rotating field machines,” *Siemens Review*, vol.34, pp.217-220, May 1972.
17. I. Takahashi, and Noguchi, “A new quick response and high efficiency control strategy of an induction motor,” *IEEE Trans. Ind. Appl*., vol.22, pp820-827, Sept/Oct. 1986.
18. Depenbrock, “Direct self control of inverter-fed induction machine,” *IEEE Trans. Power Electronics*, vol.3. no.4, pp.420-429, Otc. 1988.
19. Habetler, Thomas, Profumo, Francesco, Pastorelli, Michele, Tolbert, Leon, “Direct Torque Control of Induction Machines Using Space Vector Modulation,” *IEEE Tran. on Industry Appl.*, vol. 28, No.5, Sept/Oct 1992 pp.1045-1053.
20. Kazmierkowski, Marian and Henry Tunia, “Automatic Control of Converter-Fed Drives”, PWM-Polish Scientific Publications, Warszawa, 1994, pp 455-468.
21. Domenico Casadei, Francesco Profumo, Giovanni Serra, Angelo Tani, "FOC and DTC: Two Viable Schemes for Induction Motors Torque Control," *IEEE Trans. on power electronics*, vol. 17, No. 5, Sept. 2002.
22. Zakdy Sorchini, Philip T. Krein, "Formal Derivation of Direct Torque Control for Induction Machines," *IEEE Trans. on power electronics*, vol. 21, No. 5, Sept. 2006.
23. Jiang Zhijun, Hu Shimiao, Cao Wenhui, "A new fuzzy logic torque control

scheme based on vector control and direct torque control for induction machine," The 3rd Intetnational Conference on Innovative Computing Information and Control, Dalian, Liaoning 18-20 June 2008.

24. Shuxi Liu, Shan Li, Mingyu Wang, "An improved direct torque control of induction motor with current hysteresis band," Automation Congress, 2008. WAC 2008. World, Hawaii, HI, Sept. 28 2008-Oct. 2 2008
25. M. Farasat, N. Rostami, M. R. Feyzi, "Speed sensorless hybrid field oriented and direct torque control of induction motor drive for wide speed range applications," Power Electronic & Drive System & Technologies Conference, 17-18 Feb. 2010
26. Online source: http://en.wikipedia.org/wiki/Induction_motor.
27. Novotny, Donald and Lipo, Thomas, *Vector control and dynamics of AC Drives*, Oxford University Press, New York, 1996
28. F. Tahri, A.Tahri, Eid A. AlRadadi and A. Draou Senior, "Analysis and Control of Advanced Static VAR compensator Based on the Theory of the Instantaneous Reactive Power," presented at ACEMP, Bodrum, Turkey, 2007.
29. J. Lewis Blackburn, *Symmetrical Components for Power Systems Engineering*, Marcel Dekker, New York (1993).
30. Bahram Amin, *Induction motors: analysis and torque control*, Springer, 2001
31. Zhengshi WANG, “High Performance Computation for flux and speed estimation of vector controlled adjustable speed drives” (Hong Kong) Ph. D. Dissertation, The Hong Kong Polytechnic University 2005.
32. Rodriguez, Jose; et al., "Multilevel Inverters: A Survey of Topologies, Controls, and Applications". *IEEE Trans on Industrial Electronics* 49(4): 724–738, August 2002.
33. A.Nakagawa et al., "Safe operating area for 1200-V non-latch-up bipolar-mode MOSFETs", *IEEE Trans. on Electron Devices*, ED-34, pp.351-355(1987)
34. Online source: http://en.wikipedia.org/wiki/Inverter_(electrical).
35. Robert McDowall, Fundamentals of HVAC Control Systems, Elsevier, 2008.
36. Online source, available at http://en.wikipedia.org/wiki/Pulse-width_modulation.
37. A. M. Trzynadlowski, The Field Orientation Principle in Control of Induction

Motor, Kluwer Academic Publishers, Dordrecht, 1994.

38. Frédéric Danion, Mark L. Latash, *Motor Control: Theories, Experiments, and Applications*, Oxford University Press US. 2010.
39. Bahram Amin, *Induction Motors: Analysis and Torque Control*, Springer, 2002.
40. G. K. Dubey, Power Semiconductor Controlled Drives, Prentice-Hall, Englewood Cliffs, NJ, 1989.
41. Kedar Godbole, “Field oriented control reduces motor size, cost and power consumption in industrial applications,” Texas Instruments, 2006.
42. K. Hasse, “Dynamic of adjustable speed drives with converter-fed squirrel cage induction motors” (Germany) Ph. D. Dissertation, Darmstadt, Technische Hochschule, 1969.
43. R. D. Lorenz, “Field oriented induction motor controller for high performance applications,” *IEEE Trans, On Industry Applic.*, vol.IA-22. pp.293-297, 1986.
44. R. D. Lorenz and D. W. Novotny, “Saturation effect in field oriented induction machines,” Conference Record of IEEE IAS Annual Meeting, pp. 150-155. 1987.
45. R. Krishnan, P. Pillay, “Parameter sensitivity in vector controlled ac motor drives,” Proceedings of IEEE Industrial Electronics Conference, vol 1, pp212-218, 1988.
46. K. B. Nordin and D. W. Norotny, “The influence of motor parameter deviations in feedborward field orientation drive system,” *IEEE Trans. on Industry Applications,* vol. IA-21 pp.1009-1015, July/August 1985.
47. R. Krishman, F. C. Doran, “Study of parameter sensitivity in high performance inverter fed induction motor drive system,” *IEEE Trans. on Industry Applications,* vol. IA-23 pp. 623-635, 1987.
48. C. Wang, D. W. Novotny, “An automated rotor time constant measurement system for indirect field orientated drives,” Conference Record of IEEE IAS Annual Meeting, pp. 140-146, 1988.
49. T. Mastsuo, T. A. Lipo, “Rotor parameter identification scheme for vector controlled induction motor drives,” *IEEE Trans. on Industry Applic.* vol. IA-21, May/June 1985.
50. H. Sugimoto, S. Tamai, “Secondary resistance identification of an induction motor

applied model reference system and its characteristics," *IEEE Trans. on Industry Applications*. vol. IA-23, pp.296-303, 1987.

51. Pekka Tiitinen, "The next Generation Motor Control Method, DTC, Direct Torque Control," proceedings 1996 International Conference on Power Electronics, Drives and Systems for Industrial Growth, New Delhi, India, January 8-11, 1996 pp.37-43.
52. Salih Baris OZTURK, "Direct torque control of permanent magnet synchronous motors with non-sinusoidal back EMF" (USA) Ph. D. Dissertation, Texas A&M University 2008.
53. P. Tiitinen, P. Pohkalainen, and J. Lalu, "The next generation motor control method: Direct torque control (DTC)," EPE J., vol. 5, no. 1, pp. 14–18, Mar. 1995.
54. Barbara H. Kenny, "Deadbeat direct torque control of induction machines using self-sensing at low and zero speed" (USA) Ph. D. Dissertation, University of Wisconsin - Madison 2001.
55. Veltman, Andre, "Symmetrical Stator Flux Orbits for Direct Flux and Torque Controlled Drive," Processdings of the 1996 IEEE Industry Applications Society Annual Meeting, San Diego, CA., vol.1, pp.197-204.
56. Piotr Wach, *Dynamics and Control of Electrical Drives*, Springer. 2010.
57. Kyo-Beum Lee, Frede Blaabjerg, "Sensorless DTC-SVM for Induction Motor Driven by a Matrix Converter Using a Parameter Estimation Strategy," *IEEE Trans. on Industrial electronics*, vol. 55, No. 2, Feb 2008.
58. Joachim Holtz, "Sensorless Control of Induction Machines," Keynote Paper,
59. A. Makouf, M. E. H. Benbouzid, "A Practical Scheme for Induction Motor Speed Sensorless Field-Oriented Control," *IEEE Trans. on energy conversion*, vol. 19, No. 1, March 2004.
60. ABB Technical Guide: Direct Torque Control (Online source), Available at www.abb.com

VITA AUCTORIS

NAME: Zhi SHANG

PLACE OF BIRTH: Xi'an, Shaanxi, China

YEAR OF BIRTH: 1986

EDUCATION: Huazhong University of Science and Technology, Wuhan, Hubei, China
2005 – 2009 B.Eng.

University of Windsor, Windsor, Ontario, Canada
2009 – 2011 MASc